2019

Advanced Processing of Nickel-Titanium-Graphite Based Metal Matrix Composites

Amit K. Patil
Cleveland State University

ADVANCED PROCESSING OF NICKEL-TITANIUM-GRAPHITE BASED METAL MATRIX COMPOSITES

AMIT PATIL

Bachelor of Engineering in Mechanical Engineering

University of Mumbai

May 2013

submitted in partial fulfillment of requirements for the degree

MASTER OF SCIENCE IN MECHANICAL ENGINEERING

at the

CLEVELAND STATE UNIVERSITY

May 2019

We hereby approve this thesis

For

AMIT PATIL

Candidate for the Master of Science degree

or the Department of

Mechanical Engineering

And

CLEVELAND STATE UNIVERSITY'S

College of Graduate Studies by

_____

Dr. Tushar Borkar

_____

Department and Date

_____

Dr. Majid Rashidi

_____

Department and Date

_____

Dr. Somnath Chattopadhyay

_____

Department and Date

05/03/2019

_____

Student's Date of Defense

ACKNOWLEDGMENTS

I am extremely grateful to my advisor Dr. Tushar Borkar for his persistent support and moral assistance in research as well as academics during my master's program. I am also thankful for his guidance and endless encouragement throughout this entire research.

I would like to sincerely express my gratitude towards Dr. Majid Rashidi and Dr. Somnath Chattopadhyay for being involved in the thesis committee.

I am thankful to Dr. Rajeev Gupta from Department of Chemical & Biomolecular Engineering at The University of Akron for helping me with X-Ray diffraction characterization. Also, I would like to thank Profs. Raj Banerjee and Thomas Scharf from department of Material Science and Engineering at University of North Texas, Denton for helping me with LENS^{TM} processing and tribology test in this research.

I am forever indebted, and I must express my profound gratitude to my parents Kalyansing Patil and Vidya Patil along with my beloved brother Sagar for their support and keeping me motivated to achieve my dreams.

This work is partially supported by the National Science Foundation under Grant No. 1126126.

ADVANCED PROCESSING OF NICKEL-TITANIUM-GRAPHITE BASED METAL MATRIX COMPOSITES

AMIT PATIL

ABSTRACT

A new class of *in situ* titanium carbide (TiC)/graphite (C) reinforced nickel matrix composites with variation in composition particularly varying C/Ti ratio have been processed using two different processing techniques. Firstly, via mechanical alloying (MA) followed by spark plasma sintering (SPS), i.e. solid-state processing. Secondly, using Laser engineered net shaping (LENS^{TM}) technique, i.e. metal additive manufacturing technique. Mechanical alloying has gained special attention as a powerful non-equilibrium process for fabricating amorphous and nanocrystalline materials, whereas spark plasma sintering is a unique technique for processing dense and near net shape bulk alloys with homogeneous microstructure. Laser engineered net shaping (LENS^{TM}) is a rapid prototyping technique prominently known for its ability to fabricate full dense complex components and functionally graded materials. These composites consist of an *in situ* formed and homogeneously distributed TiC precipitates reinforcing the nickel matrix. Additionally, by tailoring the C/Ti ratio in these composites the volume fraction of TiC reinforcement can be altered, and an additional graphitic phase can also be engineered into the microstructure. These Ni-TiC-C composites exhibit excellent microhardness as well as tribological properties as compared to pure nickel. Additionally, microstructure, microhardness and tribological behavior of SPS processed Ni-TiC-C composites have been investigated and compared with LENS^{TM} processed counterparts. SPS processed Ni-Ti-C composites exhibit excellent mechanical, as well as tribological properties as compared to

LENS^{TM} processed samples primarily due to uniformly distributed refined TiC and graphite phases within nickel matrix.

TABLE OF CONTENTS

Page

LIST OF TABLES

TABLE Page

LIST OF FIGURES

FIGURE Page

CHAPTER I

INTRODUCTION

1.1. Metal Matrix Composites (MMCs)

Metal matrix composite is a class of material, consisting of a metal matrix reinforced with ceramic particulates making it suitable for numerous functional as well as structural applications.[1-3] Metal matrix composites have very high strength to weight ratio, also exhibit attractive physical and mechanical properties, superior than those of a base metal matrix, as well as ceramic reinforcement. MMCs can be used at elevated temperature due to combination of metallic properties such as high strength, modulus and ceramic properties such as high hardness and wear resistance.[1-3] The balance of such attractive properties, availability of relatively inexpensive reinforcements, various processing routes, and inherent flexibility to alter the characteristics and properties by varying the nominal compositions make it an ideal material for aerospace, energy, automotive and structural engineering applications.[1-5]

Depending upon desired application, metal matrix composites can be reinforced with ceramic particles, continuous and non-continuous fibers, or even hybrid reinforcement, consisting of both particles and fibers. Out of all these, particulate reinforced MMCs are considered as the most attractive material due to their low production

cost and their isotropic properties.[25] Generally, reinforcement particulates used in MMCs are ceramics such as metal carbides (TiC, SiC, WC, TaC), metal nitrides (TiN, TaN, ZrN, Si_3N_4), metal borides (WB, TiB_2), and metal oxides (Al_2O_3, ZrO_2) exhibiting excellent mechanical properties. These ceramic reinforcements exhibit high Young's modulus, high thermal stability, high yield strength, high hardness, high melting temperature, low density, and low coefficient of thermal expansion. These properties can be tailored with production as well as processing techniques, and with the matrix system selected in the composite materials. Out of all the ceramic reinforcement particulates, metal carbides are most commonly used primarily due to their very high mechanical strength to the metal matrix. Selection of processing routes to fabricate MMCs, mainly depends upon applications and desired properties. Factors such as size and volume fraction of the reinforcement phase and nature of the interfacial bonding between matrix and reinforcement affect the microstructure and mechanical as well as tribological properties of the composites.[6-8]

Depending on the formation of reinforcement during processing, MMCs are classified as *ex situ* and *in situ*. The first synthesis route uses a conventional technique of composite fabrication in which reinforcement are externally added to the metal matrix. Whereas, in *in situ* MMCs, formation of reinforcement takes place within the matrix. *Ex situ* has disadvantages as compared to *in situ* MMCs such as poor interfacial bond, size restriction of the reinforcement, and poor wettability, resulting in the inhomogeneous distribution of the reinforcement particulates as compared with *in situ* technique. Also, surface contamination, and particulate agglomeration can be seen in particulate reinforced *ex situ* MMCs. Homogeneous dispersion of fine and thermally stable reinforcement in the metal matrix is desirable to achieve optimal mechanical properties and enhanced

mechanical performance of MMC. Thus, the interfacial bonding between metal matrix and ceramic reinforcement need to be stable as it influences the structure and the properties of the MMC. By using the *in situ* technique of fabrication, the reinforcement is synthesized in the metal matrix during fabrication process due to exothermic chemical reaction between the constituents, thus resulting in a strong and clean interfacial bonding between metal matrix and fine scale size of reinforcement precipitates.[8,12] A more homogeneous microstructure and remarkably improved mechanical properties are achieved due to homogeneous dispersion of particles within metal matrix, control over the size, good wettability of the reinforcement particulates with the metal matrix allowing good coherency, and excellent interfacial bonding between metal matrix and ceramic reinforcement. Also, the *in-situ* reinforcement phases formed due to the chemical reaction are found to be thermodynamically stable in the metal matrix than that of *ex situ* MMCs.[7,8] Therefore due to several shortcomings of *ex situ* processing route, *in situ* processing route is most preferable for the fabrication of MMCs.

K. K. Chawla, in his work, has classified the fabrication techniques for MMCs in two categories, liquid-state processing, and solid-state processing.[36] MMCs can be fabricated using different processing techniques such as casting, forging, and powder metallurgy processing, etc. Processing routes for fabrication of MMCs play an important role in altering their microstructures, thus affecting their mechanical properties. Powder metallurgy method is most widely applied for processing MMCs, due to low cost and its inherent flexibility to alter the composition in order to get precisely tailored mechanical properties.

The size of the *in situ* formed reinforcement particles in MMCs depend on various factors such as external force, pressure and temperature during reaction, etc. Depending upon the processing temperature of the metal matrix and the reactants, S.C. Tjong has classified the Powder metallurgy process routes for *in situ* reaction into four categories: a) Solid-Liquid reaction process, b) Liquid-Liquid reaction process, c) Solid-Solid reaction process, d) Vapor-Liquid reaction process.[12] These processing routes play an important role in altering the microstructure as well as mechanical properties of the material synthesized.

In present study, Titanium carbide (TiC)-graphite(C) reinforced Nickel matrix composites were fabricated by powder metallurgy technique using solid-solid and solid-liquid reaction process. Mechanical alloying (MA), which falls under solid-solid reaction process is a solid-state processing method and was used for *in situ* formation of reinforcement phase which was later consolidated using spark plasma sintering (SPS). In solid liquid reaction process, the reinforcement phase is formed in the matrix solvent via diffusion reaction. Laser Engineered Net shaping (LENS^{TM}) technique was used in this study for fabrication of MMCs using solid-liquid reaction process. In both processing routes, *in situ* MMCs have been processed using elemental blend nickel, titanium, and graphite powder particles.

1.2. Objectives

A. Fabrication of Ni-TiC-C composites with variation in volume fraction of *in situ* formed reinforcement precipitates using SPS and LENS^{TM} processing techniques.

B. Identify and study the phases evolved during the processing.

C. Study the difference in the microstructure and the reinforcement distribution achieved after fabrication using two different techniques.

D. Observe the effect of volume fraction of reinforcement on microstructure, microhardness, and tribological performance of the composites.

E. Comparing two different processing techniques based on the derived results.

1.3. Organization of thesis

There are total five chapters in the thesis. The first chapter deals with brief review of Metal matrix composites, its application and classification, and fabrication techniques. It also provides information on the objective of the present work and further organization of this thesis.

Chapter two describes the processing techniques utilized in the present work for the fabrication of metal matrix composites and provides information on purpose of selecting Ni-Ti-C ternary system for this investigation, describing its remarkable properties and significance importance. It also shares the previous research work carried out in relevant area in the form of literature review.

Chapter three deals with experimental procedures along with the process parameters used to synthesize Ni-TiC-C composites using two different processing techniques i.e. mechanical alloying followed by SPS and LENS^{TM}. Later, it describes the characterization techniques involved and the apparatus used for it.

Chapter four describes the results and discussion based on the processing routes as well as characterization techniques used and mentioned in previous chapters. This chapter concludes with comparing microstructure, mechanical, and tribological properties of Ni-TiC-C composites processed via SPS and LENS^{TM} processing routes.

Lastly, chapter five summarizes the results and concludes the present work.

CHAPTER II

METHODOLOGY

This chapter provides understanding on the methods and processing techniques utilized for the fabrication of metal matrix composites in the present work and highlights the importance of mechanical alloying (MA), spark plasma sintering (SPS), laser engineered net shaping (LENS^{TM}), and Ni-Ti-C ternary system used in this study. Furthermore, it also provides brief literature review on the research work previously carried out in relevant area.

2.1. Powder metallurgy

Powder metallurgy process is known for its rapid production method of accurately fabricating components and offers control over the microstructure and characteristic properties. Powder metallurgy offers precision and flexibility to control the features and the characteristics of the part fabricated, which is very difficult or near impossible to achieve using any other conventional processing techniques. It also eliminates additional machining operations as involved in casting, and other traditional techniques to achieve final dimension.[28]

The powder metallurgy technique has an excellent set of advantages such as it enables efficient material utilization and fabrication of complex components with near net

shape possible, fabrication of components using hard materials such as WC, TiC, and components can be fabricated in pure form as the purity of precursors used gets preserved throughout the process. It also makes utilization of wide variety of materials such as metals, alloys, ceramics and other immiscible systems possible.[29]

The recent development in powder metallurgy has helped in developing novel alloys with better mechanical properties in order to crater the current industrial demands. It has also boosted and helped in development for the wide spectrum of additive manufacturing techniques. Powder metallurgy technique has helped manufacturing of pre alloyed powders which can be used by additive manufacturing process for the fabrication of complex components with improved mechanical performance. Powder metallurgy process has opened new routes to process advanced materials with controlled microstructure using processes such as mechanical alloying and rapid solidification processing (RSP).

2.2. Mechanical Alloying

Mechanical alloying (MA) is an effective solid-state powder processing technique permitting the development of refined microstructure and nanocrystalline size of homogeneously dispersed *in situ* reinforcement which improves the mechanical properties of the composite while retaining the ductility of the metal matrix.[12,13] Mechanical alloying is a unique process allowing the production of advanced materials, which was difficult or impossible to fabricate with traditional techniques.

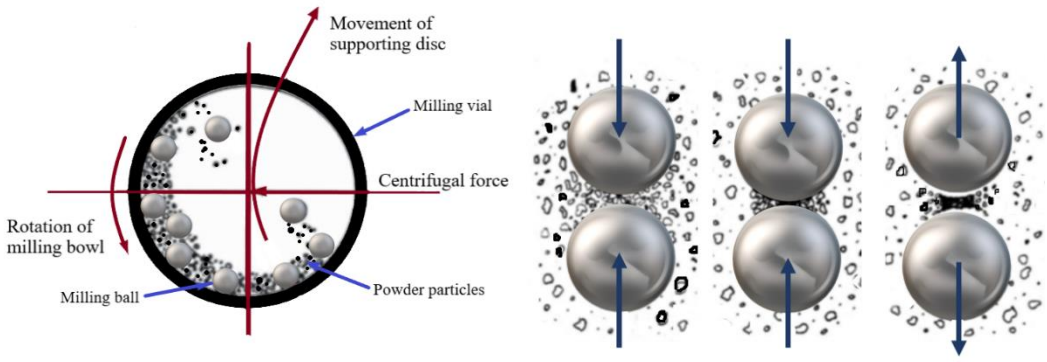

Figure 1. Schematic of mechanical alloying kinematics and mechanical alloying process

It is a mechanochemical process by which *in situ* ceramic reinforcement can be induced in the composite via mechanically activated chemical reaction using elemental powders. It has been showed that *in situ* formation of composites leads to better properties in comparison with conventionally synthesized composites.[30,31] The process starts with the blending of elemental powder in required proportion and is subjected to high energetic compressive impact forces in a mill using grinding media until a steady state is achieved. MA is considered as a complex stochastic process having numerous independent and interdependent process variables involved and depend on factors such as the desired phases, microstructures, and properties. Depending upon these factors, selection and optimization of these variables are required in order to obtained MMCs with desired properties.[13] MA has been proven capable of processing a wide variety of materials such as intermetallic alloys, Ceramics, and other refractory materials. Both miscible and immiscible systems material systems can be processed using MA. Mechanically alloyed materials possess high strength and are found to be stable at both room temperature and elevated temperature.[13]

C Suryanarayana reported that during MA, repetitive fracturing, cold welding and rewelding governs the shape and size of the milled powders which increases the wettability and results in better dispersion of reinforcement in the metal matrix by breaking up the ceramic clusters.[13] Previous studies have indicated that particle size has significant influence on the recrystallisation process affecting grain size and microstructure of the sintered composites.[13-15] It is well known that grain size refinement of metallic materials to nanoscale enhances mechanical properties such as strength and hardness of the material maintaining the original ductility.[24] Hall-Petch relationship states that grain size has a great influence on the composite strength as they as it acts as a pinning point and hinders the dislocation movement.[59] Thus, ball milling was performed to reduce the particulate size and for homogeneous dispersion of the *in situ* reinforcement precipitates within the metal matrix.

2.3. Spark Plasma Sintering (SPS)

Spark plasma sintering (SPS) also known as Field assisted sintering technique (FAST) is a novel consolidation technique suitable to sinter metal, alloys and composites at relatively low temperatures below their melting point and shorter sintering time compared to the conventional techniques. It has a high heating rate, shorter holding time, and low sintering temperature which retards the grain growth retaining refined microstructure and increases the microhardness as well as mechanical properties of the composites.[16-19,47] In SPS, consolidation of powder is taking place due to microscopic discharge of pulsed direct current between particles under uniaxial pressure, promoting densification during sintering. Melting of the surface of the powder takes place due to resistive joules heating effect energized by DC pulsed electric current.[20,21]

The composite samples processed via SPS technique can achieve full densification, and grain growth can also be avoided due to rapid heating up to 1000^{o}C/min as well as shorter holding time. This ability to reach the processing temperature in a short duration of time due to high heating rate, minimizes the processing time required for sintering.[48,49] In SPS process, part porosity can be controlled by changing the processing parameters such as applied pressure, holding time and processing temperature.[50] In SPS, sintering takes place in shorter cycle time; thus, limiting grain growth and preventing undesired phase transformation or intermetallic reaction of the material during processing. The SPS technique also possesses numerous other advantages. For example, it is less sensitive to initial material characteristics, it can consolidate difficult to sinter material, no need of sintering aids, no cold compaction required before sintering as needed in other techniques and helps achieving improved characteristic properties of the consolidated material. These

outstanding advantages make the SPS process preferable over other conventional techniques of sintering.[51]

The material sintered using SPS process can be both conductive and non-conductive. Conductive material is heated by resistive joules heating effect and by heat transfer from the die. Whereas, in case of non-conductive material, heating takes place only through heat transfer from the die.[51] Previous work has demonstrated that a wide variety of conducting or insulating materials such as metals, ceramics, and composites can be processed using the SPS technique.[47-49]

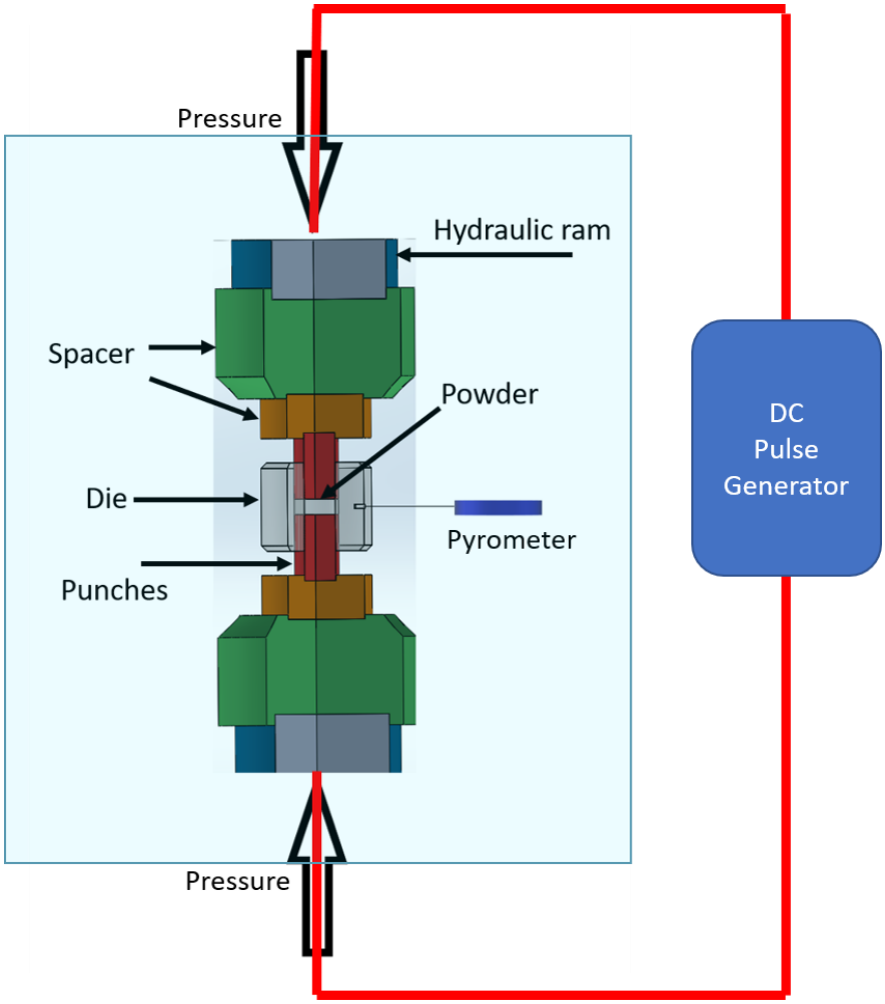

Figure 2: Schematic illustration of the SPS system

Figure 2. shows schematic of SPS system. In the SPS technique, the powder to be sintered is placed in a graphite die when low pressure, typically less than 100MPa is applied. However, if the applied pressure is more than 100MPa, tungsten carbide die is used. Graphite foil is used inside the die and in the assembly to improve the conductivity. Die and Punches of the same material are used. Uniaxial pressure is applied with the help of plungers, blocks, and cold spacer assembly, requiring all of them to be electrically conductive. Generally, graphite, stainless steel, or copper is used in the assembly.[51,53] If the applied pressure is less 100MPa, graphite is most preferred due to its high thermal conductivity.

In this process, the powder particles are sintered due to the surface evaporation and melting of the powder surface followed by solidification during cooling. Due to microscopic discharge of pulsed DC current between particles, a local high temperature state of several hundreds to thousands of degrees centigrade is formed. This high temperature causes evaporation and melting on the surface of the powder particles and neck formation around the contact area between the particles takes place. Also, the flow of material due to plasticity and under applied pressure brings particles together and promotes necking. This processing phenomenon under applied pressure, allows sintering through SPS at lower temperatures as compared with other processing techniques.[51,52] The amount of current required during the SPS cycle depends on factors such as die geometry, processing temperature, conductivity of the material processed, etc. For high heating rates, large sizes of die, and high processing temperature, a higher current is required. In present study, SPS 10-3 by Thermal Technologies was used. This system can apply up to 10000

kg of pressure, 3000 Amps and 10 volts of current. Generally, the pulse DC signal is ON for 30ms, and OFF for 2ms

Several research works were carried out on fabrication of *in situ* MMCs via SPS preceded by high energy mechanical alloying using ball mill and a substantial improvement in mechanical properties particularly, in terms of mechanical strength, wear resistance, hardness, thermal conductivity was observed. It was also noticed that even after consolidation, the nanocrystalline size obtained via MA was preserved. [25,27,34]

Currently, the industrial application is limited to the area where it is difficult to process high performance materials using traditional techniques. Also, further machining is required for the material consolidated through the SPS process but still you can get near-net shape.

2.4. Laser Engineered Net Shaping (LENS^{TM})

Laser Engineered Net Shaping (LENS^{TM}) is an additive manufacturing technique first developed at Sandia National laboratory in the United States and was subsequently commercialized by Optomec Inc. It is a directed energy deposition technique and solid metal forming process for the fabrication of 3d components. Due to its rapid cooling and high solidification rate, it is advantageous in achieving homogeneous as well as refined microstructure with improved mechanical properties as compared with other conventional methods. LENS^{TM} is an additive manufacturing technique prominently known for its ability to fabricate full dense, complex components as well as functionally graded materials.

Application of LENS^{TM} technique includes rapid prototyping, low volume manufacturing, and product development for aerospace, medical and defense industries, and surface engineering applications. This technique has the flexibility to deposit material on existing or pre-deposited, makes it possible to repair. Material restrictions, such as it can only use spherical metal powders with a size range of 50µm – 150µm is used as a raw material for fabrication.[37] Unlike other rapid prototyping techniques, no plastic-coated materials, filler materials, or binders is required in this processing technique. The fabrication of component takes place under controlled inert Argon environment in the hermetically sealed glove box with oxygen content as low as 10ppm, to prevent contamination, and avoiding the formation of any undesired intermetallic phases. Figure 3. depicts the working schematic of LENS^{TM} process.

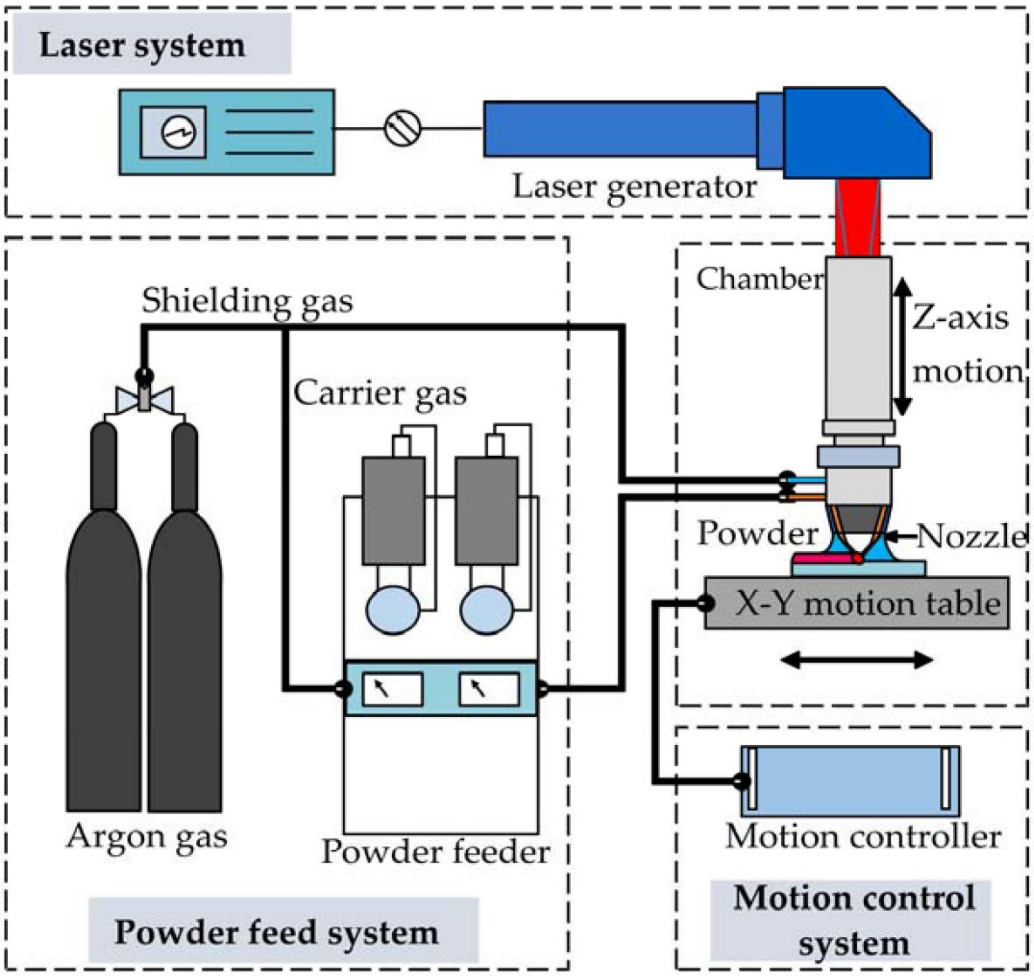

Figure 3: Schematic illustration of the LENS^{TM} system[54]

Depending on the material to be deposited, and power output required, Nd-YAG or fiber laser can be used to process various types of elemental powders. It has a four co-axial nozzle powder feeder system; it is designed in such a way that all the nozzles are focused at a point where the laser beam is focused. Delivery of elemental powder from the powder hoppers through the nozzle is carried out with the help of inert gas delivery system. The high-power density from the focused laser beam generates a melt pool on surface of the substrate or previously deposited layer. The substrate is moved relative to the laser beam to deposit thin layers of controlled width and thickness. The movement of the substrate and the flow rate of powder is controlled by the control system. Powder through the delivery

system is sprayed and absorbed in the melt pool. Due to small melt pool geometry and rapid cooling rate, this component fabricated using this component has very fine refined microstructure with fine grain size.[38,39] Materials such as stainless-steel alloys, tool steel alloys, titanium alloys, nickel and nickel based super alloys, cobalt alloys and other composite materials have been fabricated via LENS™.

LENS™ system uses multiple hoppers for powder feeder which add to its flexibility and make it possible to fabricate compositional graded components. This ability makes it possible for deposition of functionally graded materials (FGMs). FGMs are advanced materials, whose composition and the microstructure change gradually from one direction to other. Its main characteristic is its graded composition and microstructure, resulting in variation of properties. This tailored composition and microstructure of the components, helps in achieving distribution of properties as desired for wide range of applications. [40,41] FGMs can be processed via several methods such as CVD, Plasma spraying, Powder Metallurgy, SHS, LENS™, etc. But due to limitation of shape and size of the die in pressure aided sintering. LENS™ process is most suited for the fabrication of FGMs.[42]

Some examples of previous work carried out on fabrication of MMCs using LENS™ and demonstrating its efficacy, includes laser based fabrication of IN625 based MMCs with Ni-coated and uncoated TiC particles as reinforcement by Zheng *et al*.[43], WC-Co cermets fabricated by Xiong *et al*.[44], Liu *et al* worked on fabrication of FGM TiC/Ti composites using LENS™ process[42], deposition of Ti-6Al-V4 using LENS™.[46]

2.5. Nickel-Titanium Carbide-Graphite

Nickel exhibits various attractive properties such as excellent corrosion and wear resistance, ductility, toughness and has a low coefficient of thermal expansion. Owing to its properties such as heat resistance, resistant to fatigue and abrasion, resistant to oxidation and its ability to retain its shape and strength even at high temperature, nickel and nickel-based superalloys has been widely used in aerospace, petrochemical industry and numerous other processing industries.[7,8] Nickel based MMCs with ceramic reinforcement are used for various industrial applications including operations involved with cutting, stamping, punching, rolling, piercing, etc.[3]

Titanium Carbide (TiC) is a refractory material with excellent combination of properties such as high hardness of 3200 (HV), high Young's modulus (440 GPa), low density (4.93 g/cm^3), low coefficient of friction, excellent corrosion and wear resistance, high melting point (3200^{0}C), resistant to abrasion, and infusibility. These remarkable properties make TiC an ideal candidate as ceramic reinforcement adding high mechanical strength to the metal matrix.[7-12]

TiC has high hardness value but is extremely brittle thus cannot be used as monolithic ceramic for direct engineering application. Therefore, TiC is a prominent reinforcement material in ductile and tough Nickel base metal matrix and makes an excellent hybrid material for automotive, petrochemical, aerospace and high-temperature structural applications where high compressive strength, low coefficient of friction, and high wear resistance are required at elevated temperatures. It is also known that as compared to other metals, nickel exhibits a low wetting angle with Titanium carbide, thus leading to an improved interfacial bonding in TiC reinforced nickel matrix.[7] Nickel has

very less affinity towards carbon, so it does not form an equilibrium carbide phase which makes it a suitable metal matrix for TiC reinforcement. Moreover, TiC being chemically inert it does not undergo phase transformation and it is thermodynamically stable in metal matrix.[10,11] TiC is the hardest of all metal carbides, it is 33 percent harder and has very low density in comparison with Tungsten carbide (WC).[26] These combined properties of TiC reinforced with nickel matrix makes it potential replacement for WC based materials for structural applications where high wear resistance, and low density is desired. Thus, the combination of Ni and TiC was selected for the MMC due its significant importance in plenty of industrial applications because of its remarkable properties. Also, by altering C/Ti ratio in Ni-TiC-C composites an additional graphite can also be engineered in the microstructure. Additional Graphite phase shows lower shearing strength under friction thus it remarkably increases solid lubrication and reduces coefficient of friction making it significantly promising for surface engineering application.[7,8]

Previously many researches were conducted extensively on fabrication of *in situ* formed TiC reinforcement in Nickel metal matrix to attain optimal mechanical properties and to envisage its potential applications. It emphasized on the optimization of the mechanical properties of nickel using TiC as reinforcement precipitates.[7-9,12,34]

J. Zhuang. *et al*. in his research utilized MA and SPS to synthesize Titanium Carbide reinforced Copper matrix composites and efforts were made to study its influence on dry sliding wear behavior. It was reported that addition of TiC reinforcement in Cu matrix, substantially reduced the coefficient of friction and improved wear resistance.[27] K. Ravi *et al*. synthesized Aluminum matrix composites reinforced with TiC using stir casting method and found that addition of TiC in Aluminum alloy increased hardness,

density and tensile strength of the composite. They have noticed that hardness of composite increased further with increase in TiC particles.[33] Y. Li *et al*. have studied the effects of TiC content in Ni-TiC matrix processed using Direct Laser Fabrication technique and found increase in microhardness and improved microstructure due to presence of *in situ* formed hard TiC precipitates.[32] S. Zohari *et al*. utilized MA and SPS to fabricate *in situ* Ni-TiC nanocomposite clad layer on st37 steel substrate and found enhancement in hardness and density due to *in situ* processing technique.[34] Recently, B. AlMangour *et al*. studied *in situ* reinforcement of TiC particle in stainless steel matrix using MA followed by selective laser melting technique and found that a continuous, well hardened tribolayer demonstrated the enhanced wear resistance.[35]

In this study, efforts have been made to fabricate Ni-TiC-C composites of various C to Ti stoichiometric ratio using two different processing techniques. Firstly, using Mechanical alloying of Ni-Ti-C powder followed by consolidation using Spark plasma sintering. Secondly, using Laser engineered net haping (LENS^{TM}) process. Several different compositions of Ni-TiC-C metal matrix composites were sintered, with varying the C/Ti ratio in order investigate effect of volume fraction of TiC reinforcement and graphite phase on the microstructures, mechanical, and tribological properties of these composites.

CHAPTER III

EXPERIMENT METHODS

3.1. Processing using Mechanical alloying followed by Spark Plasma Sintering (SPS)

Elemental powders of Nickel (3-7 μm, 99.9% pure), Titanium (-325 mesh, 99.5% pure) and Graphite (-325 mesh, 99% pure) were selected as a starting precursor. These powders were sourced from Alfa Aesar. Samples were stoichiometrically mixed in several different nominal compositions with varying atomic weight percentage of Nickel, Titanium, and Graphite as shown in Table I. The blend of these elemental powders was then mechanically alloyed using high energy ball milling (HEBM) equipment.

For brevity, the powders mixed with the nominal composition 80at%Ni-10at%Ti-10at%C is further referred as Ni-10Ti-10C. Similarly, this will be followed for all other Ni-Ti-C composites. The compositions with varying atomic weight ratio of Carbon to Titanium (C/Ti) are listed in Table I.

Sr. No.	Sample	Nickel (at%)	Titanium (at%)	Carbon (at%)	C/Ti
1.	Pure Ni	100	-	-	-
2.	Ni-10Ti-5C	85	10	5	0.5
3.	Ni-10Ti-10C	80	10	10	1
4.	Ni-5Ti-10C	85	5	10	2
5.	Ni-7Ti-20C	73	7	20	2.86
6.	Ni-6Ti-20C	74	6	20	3.33
7.	Ni-5Ti-20C	75	5	20	4
8.	Ni-4Ti-20C	76	4	20	5
9.	Ni-3Ti-20C	77	3	20	6.66

Table I: Nominal composition of SPS processed sample in atomic weight percentage

Planetary micromill FRITSCH Pulverisette 7 premium line which is a planetary ball mill was employed for mechanical alloying with 3 mm diameter Tungsten carbide (WC) milling media with Ball to Powder weight ratio (charge ratio) of 15:1. Samples were ball milled at 600 rpm for 24 hours in 80 ml Tungsten carbide grinding bowl. To avoid cross contamination of the milled powders grinding vessel and grinding medium of same material were selected. In order to prevent excessive temperature rise during milling, 60 mins of milling was followed by cooling interval of 30 mins. Mechanical alloying was performed under inert argon gas atmosphere to prevent oxidation of powder. 2 wt % of the total powder charge of stearic acid ($C_{18}H_{36}O_2$) was used as a process control agent in order to prevent excessive cold welding of these powder during ball milling.

The as milled powders were then sintered using spark plasma sintering technique. SPS 10-3 by Thermal Technologies LLC was used for sintering of mechanically alloyed *in*

situ Ni-Ti-C composite powder. The SPS process was programmed by specific sets of operation instructions such in the software, ITools. Set points for temperature, applied force with rate, heating rate, dwell time, ramp up/ramp down time were assigned in the program.

The sintering process was carried out at 1100^0C with a heating rate of 100 ^{0}C/min under maximum uniaxial pressure of 50 MPa with dwell time of 5 minutes. A cylindrical graphite die of 20mm inner diameter was used. An optical pyrometer was used to yield the temperature inside the die.

The SPS consolidated samples were mounted on graphite based conductive resin at 359^OF under 4000 psi. The mounted samples resulted into one and quarter inch specimen, making it easier to hold and polish the sample. The mounted samples were then mechanically polished using abrasive silicon carbide (SiC) paper having high friability to remove external graphite layer. The samples were polished sequentially using 240, 400, 600, 800 and 1200 grit SiC paper. Polishing was carried out under constant supply of water for cooling and removal of debris. Final lustrous metallographic finish was achieved by polishing using micro-cloth and 0.04μm colloidal silica solution. The samples were then washed in an ultrasonicate using soap solution, water and ethanol rinse each respectively for microstructural characterization.

3.2. Processing using Laser engineered net shaping (LENS^{TM})

Elemental powder of Nickel (40-150 µm), Titanium (40-150 µm) and nickel coated graphite powders (which can pass through -300/ +325 mesh) were selected as starting powder. These powders were sourced from Alfa Aesar. All the powders were gas atomized. The powders were stoichiometrically mixed in several different nominal compositions with varying atomic weight percentage of nickel, titanium, and graphite as mentioned in Table II.

Sr. No.	Sample	Nickel (at%)	Titanium (at%)	Carbon (at%)	C/Ti
1.	Pure Ni	100	-	-	-
2.	Ni-10Ti-5C	85	10	5	0.5
3.	Ni-10Ti-10C	80	10	10	1
4.	Ni-7Ti-20C	73	7	20	2.86
5.	Ni-3Ti-20C	77	3	20	6.66

Table II: Nominal composition of LENS^{TM} processed sample in atomic weight percentage.

It is well known that variation in flow rate of powder is possible due to differences in the density and irregularity in the surface. It has also shown that metal coated powder particles improved flowability and the powder feeding, which was mainly due to increased particle density, and smoother surface of the particle. [43] Thus, to avoid the flow variation of the powders, nickel coated graphite powder was used instead of pure graphite powder. Nickel coated graphite powder used had composition of 75wt% of C and 25wt% of Ni. Four different nominal compositions with varying atomic weight percentage of nickel, titanium and nickel coated graphite were stoichiometrically mixed twin-roller mixer. Twin-roller mixer consist of two rollers moving in opposite direction. The powders were mixed

for 6 hours at 300rpm in order to achieve near homogeneous mixture. The powder mixture was then loaded in the powder feeder of the LENS^{TM} system.

Similar to other additive manufacturing technology, LENS^{TM} process also begins with computer-aided design (CAD) file of a three-dimensional component to be fabricated. Fabrication is carried out by layer by layer deposition of the component on a nickel substrate. Using the powder delivery system, the homogeneous mixture of powder was ejected through the nozzle at a focused point which converges at a point where the high-power laser beam is focused. In this experiment, a high powered 500W Nd: YAG laser emitting near infrared laser radiation at a wavelength of 1.064μm was used. The Laser beam was focused to create a melt pool of powder ejected on a substrate with the help of inert argon gas flowing through a four-nozzle assembly. Subsequently, the substrate is moved relative to the laser beam to deposit thin layers of controlled width and thickness. Scan speed of 10 inches/min and hatch width of 0.018 inch and a layer thickness of 0.01 inch was used during the deposition. The layer deposition is carried out in a controlled inert argon gas environment in the hermetically sealed glove box. The argon gas is continuously recirculated at a flow rate of 3 liters/min throughout, and the oxygen content was maintained below 10 parts per million (PPM) during deposition.

The *in situ* composites were deposited on the substrate in a cylindrical geometry of diameter 10mm and height 10mm. These deposited composites were taken out from the glove box through the anti-chamber present in the LENS^{TM} system to avoid any atmospheric oxygen contamination and were cut from the nickel base plate using electric discharge machine. (EDM). These samples were then mounted and mechanically polished, using same procedure as described in the previous section.

3.3. Characterization of Ni-Ti-C composites

3.3.1. X-Ray diffraction (XRD)

X ray diffraction technique was used to identify the phases present in the composite samples. It works on the principle of Bragg's Law, given by $n\lambda = 2d\sin\Theta$

Where, n= Integer determined by the given order, λ= Wavelength of the radiation in angstrom (Å), d= Interplanar spacing in angstrom (Å), Θ= Angle of diffraction in radians.[60]

The radiations from the emitter are reflected at different planes at different angles with variation in intensity which is detected by the detector. The emitter and detector are rotated with variation in angle to complete a full scan of the sample, some of the incident rays are reflected off the first atomic plane while some rays are reflected from the adjacent atomic plane as shown in Figure 4.

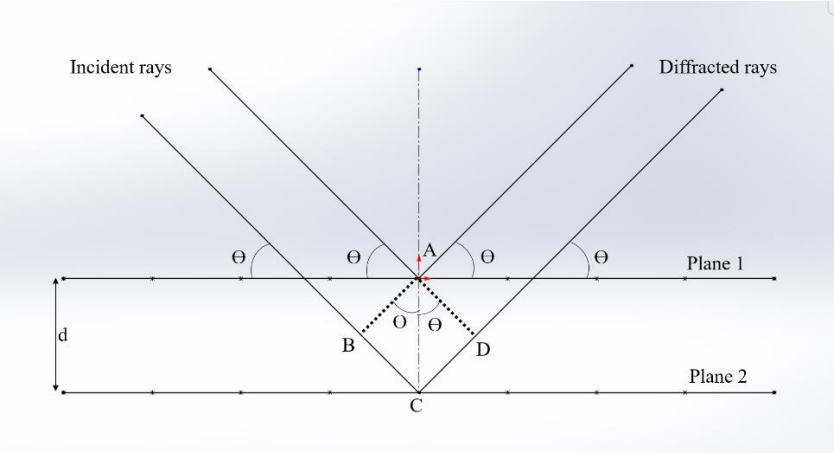

Figure 4: Schematic illustration of Bragg's Law

When the incident radiations are reflected from different planes meets each other, constructive or destructive interference takes place. If the interference is destructive, it will reflect low intensity and a flat line will appear. Constructive interference will occur when

a full phase shift in the rays takes place that is when the sum BC+CD is an integer and the Bragg's law fits true. In case of constructive interference, it will reflect an intensity peak in XRD profile. Constructive interference occurs only at specific angles, depending upon crystallography.[60] These specific angles reveal the crystal structure of the phases present in the sample. The results after analyzing the data determines hkl values of the crystal planes. The X-ray diffraction data is plotted between the intensity (arbitrary units) of the peaks versus the diffraction angle which was measured in 2Ɵ (degree).

In this experiment, tests were carried out in Rigaku SmartLab X-ray diffractometer. XRD analyses was performed employing monochromatic Cukα radiation generated at 40 KV with a wavelength of 1.5402Å.

Following parameters were used to collect the data:

scan speed: 1.0 deg/min; step width: 0.04 deg; scan range: 20deg – 100deg

3.3.2. Scanning electron microscopy (SEM)

Additional characterization was done to observe the microstructure, phases and study the effect of the processing techniques used, the composite samples processed using SPS and LENS^{TM} techniques were analyzed using scanning electron microscope (SEM). Inspect F50 from FEI Corporation was used in obtaining secondary and backscattered micrographs to investigate the morphology as well as phases present in these composites, and to identify the effect of SPS and LENS^{TM} processing technique on their microstructure.

3.3.3. Vickers Microhardness

Vickers microhardness was determined using Wilson VH1202 hardness tester from Buehler having an accuracy of ±1.5%. Microhardness was evaluated under test force of 0.5 kgf and dwell time of 10 seconds as recommended by ASTM E384 standards. A pyramid shaped diamond indenter was used for indentation. Indent diagonals were measured using the measurement system in the Wilson DiaMet and the Vickers microhardness number was calculated for the load and indent dimensions.

Vickers hardness number (VHN) is calculated using equation mentioned below,

$$VHN = 2P\sin(\alpha/2)/d^2 = 1.854P/d^2$$

Where, P is the test force in gram-force, d is the average of the diagonals of the indentation in μm, α is the indenter tip angle which is taken as 136^{o}.[61]

The test was carried out according to ASTM E384 standards. Test was performed under ambient conditions and at least ten readings at different position were taken for each sample.

3.3.4. Tribology

The dry sliding wear tests of the processed samples were conducted using Falex ISC-200 Ball-on-disc system by Implant Sciences. Testing was carried out at room temperature. Tests were performed under a normal load of 100g (1 N). The load (N), sliding speed, and track radius is kept constant throughout the test. Coefficient of friction was obtained from the ratio of tangential load to normal load. To show steady-state friction

behavior, tribological test was carried out in dry sliding conditions with sliding distance of 140m for each sample.

3.3.5. Energy Dispersive Spectroscopy

EDS characterization technique is a chemical analyzation technique used along with SEM to identify the unknown material from its elemental phases and its relative proportion present in the sample. This technique was used identify the phases and the composition of the composite samples.

CHAPTER IV

RESULTS AND DISCUSSION

4.1. SPS processed Ni-Ti-C composites

4.1.1. X-Ray diffraction analysis

X-ray diffraction patterns for SPS processed Ni-Ti-C composites are shown in Figure 5. From these patterns it is apparent that, Ni (FCC), TiC (NaCl-FCC) and C (HCP) are the only principal phases present in these composite samples indicating no undesired intermetallic phases or impurities were present in the sample. Absence of any peaks corresponding to NiTi intermetallic phase shows no reaction between Nickel and Titanium. Peaks corresponding (111), (200), and (220) crystallographic planes of FCC nickel, whereas peaks corresponding (111), (200), (220) and (311) crystallographic planes of FCC titanium carbide phase were observed at the position which agrees with the X-ray diffraction data files of pure nickel and TiC.[58]

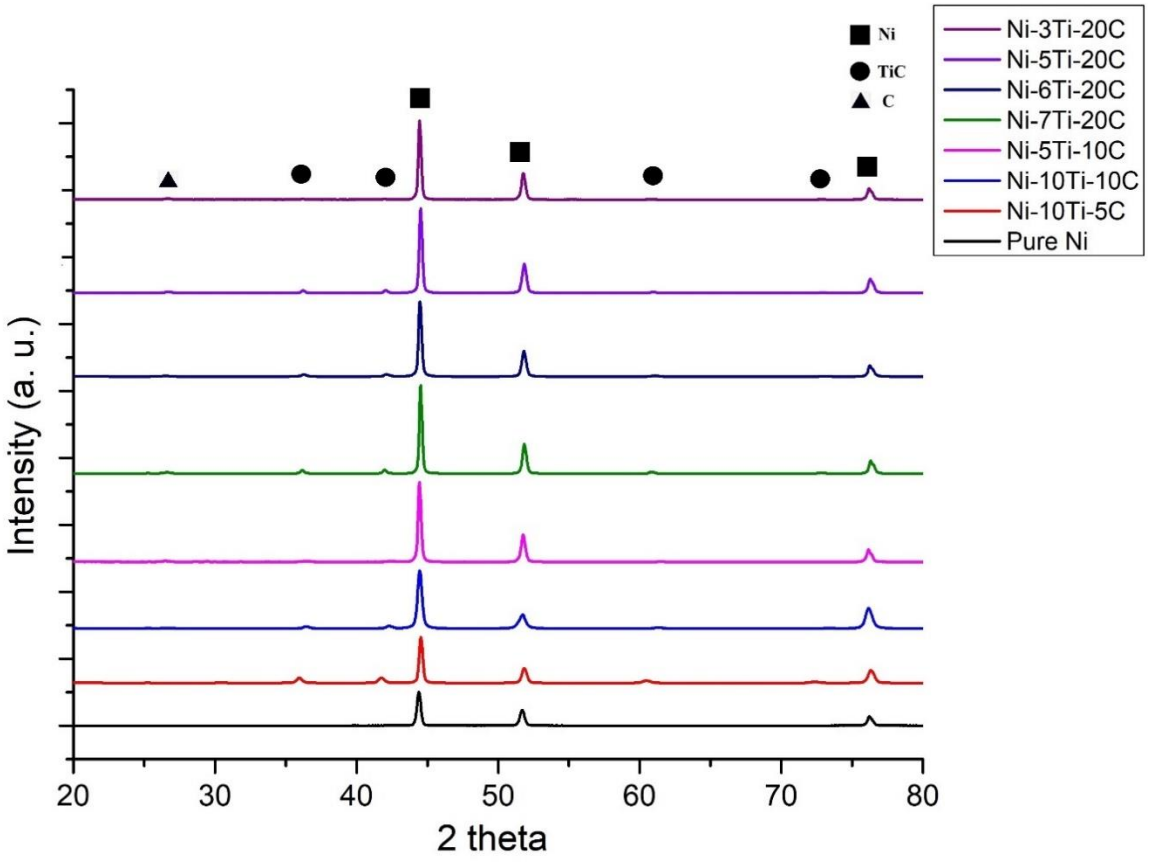

Figure 5: XRD pattern for SPS processed samples

From the characteristic peaks of TiC phase with FCC Bravais lattice, it is apparent that Titanium and graphite have undergone an *in situ* reaction in order to form titanium carbide (TiC). It also indicates the stability of TiC in the nickel matrix. Figure 5. Indicates that Ni-10Ti-5C and Ni-10Ti-10C exhibited highest intensities for TiC peaks as compared to other Ni-Ti-C composites. This increase in intensity of TiC peak in these composites are primarily due to large volume fraction of TiC precipitates present in these composites.

In XRD analyses result, the presence of hcp (0002) carbon peak at ~26^0 in the XRD pattern confirms the presence of Graphite phase in the composites. It is possible to engineer an extra lubricious graphite phase by altering the C/Ti ratio. Also, intensity of (0002) carbon peak increases with increasing C/Ti ratio, as carbon does not have solubility with

nickel and there is not much titanium available to react and form TiC. It was observed that with increasing C/Ti ratio, the intensity of peak increases but later it decreases with increase in intensity of (0002) Carbon peak as the C/Ti ratio increases further beyond 1.

4.1.2 Microstructural Analysis

The microstructural analysis of pure nickel and Ni-Ti-C composite samples were characterized under FEI Inspect F50 equipped with backscattered electron detector.

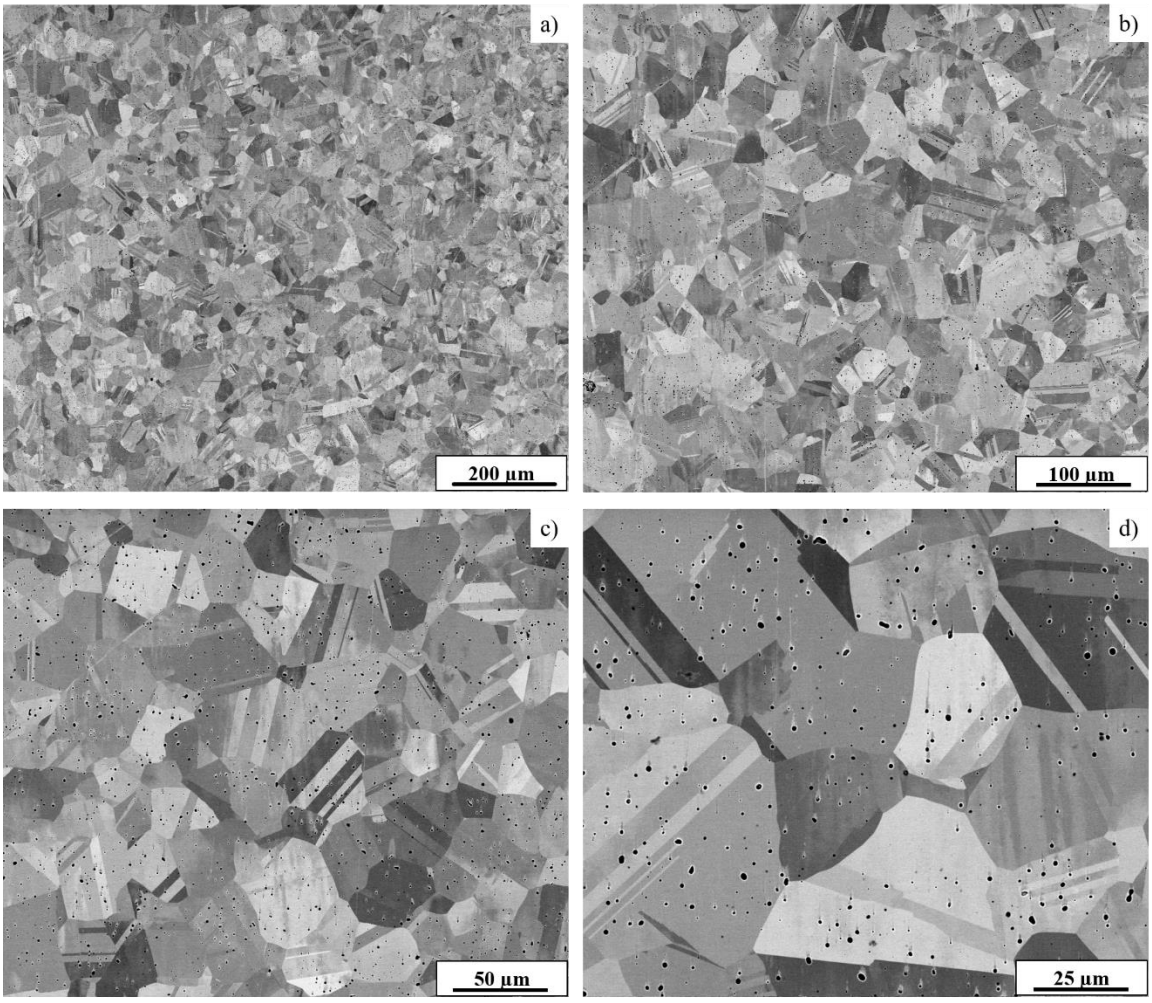

Figure 6: Backscattered images of Pure Ni at a) 250X, b) 500X, c) 1KX, d) 2KX magnification

Figure 6. shows SEM images of SPS processed pure nickel sample. Pure nickel exhibits randomly oriented grains along with annealing twin boundaries which are clearly seen in Figure 6. These annealing twins were formed due to relatively low stacking fault energy of nickel thus reducing the total interfacial energy of the system. Also, the grain size of pure nickel was observed in few microns ranging between 15µm to 30µm.

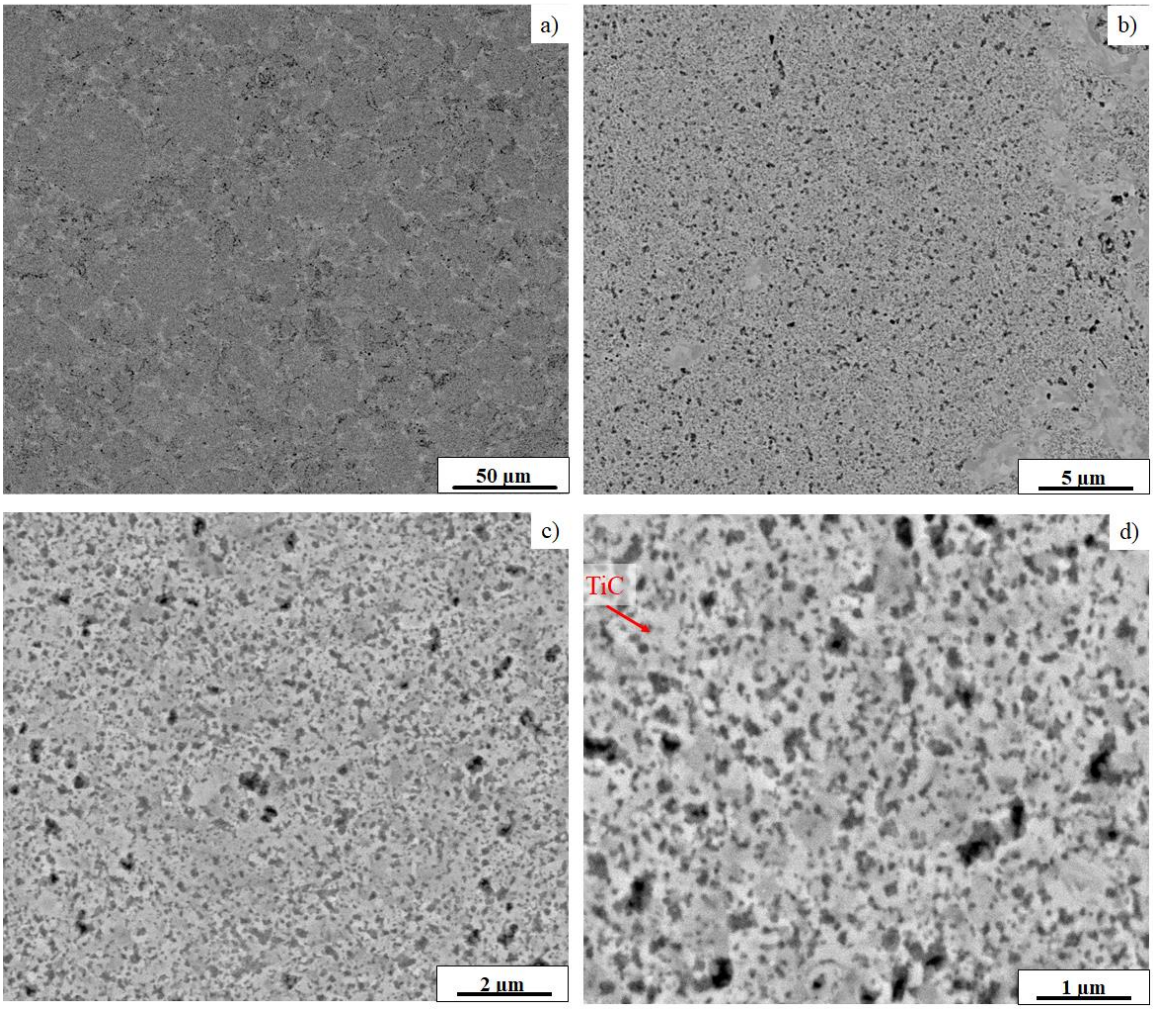

Figure 7: Backscattered images of Ni-10Ti-5C at a) 1KX, b) 10 KX, c) 25KX, d) 50KX magnification

SEM images of SPS processed Ni-10Ti-5C are shown in Figure 7. It can be seen clearly from the micrographs that nanosized TiC precipitates exhibiting spherical morphology are homogeneously distributed within the randomly oriented nickel grains. These uniformly distributed TiC precipitates help in retaining the refined nickel grains by obstructing their grain growth during SPS processing. These uniformly distributed hard TiC precipitates along with refined nickel microstructure contributes to the increase in hardness of the composite by obstructing grain boundary dislocations during plastic deformation.

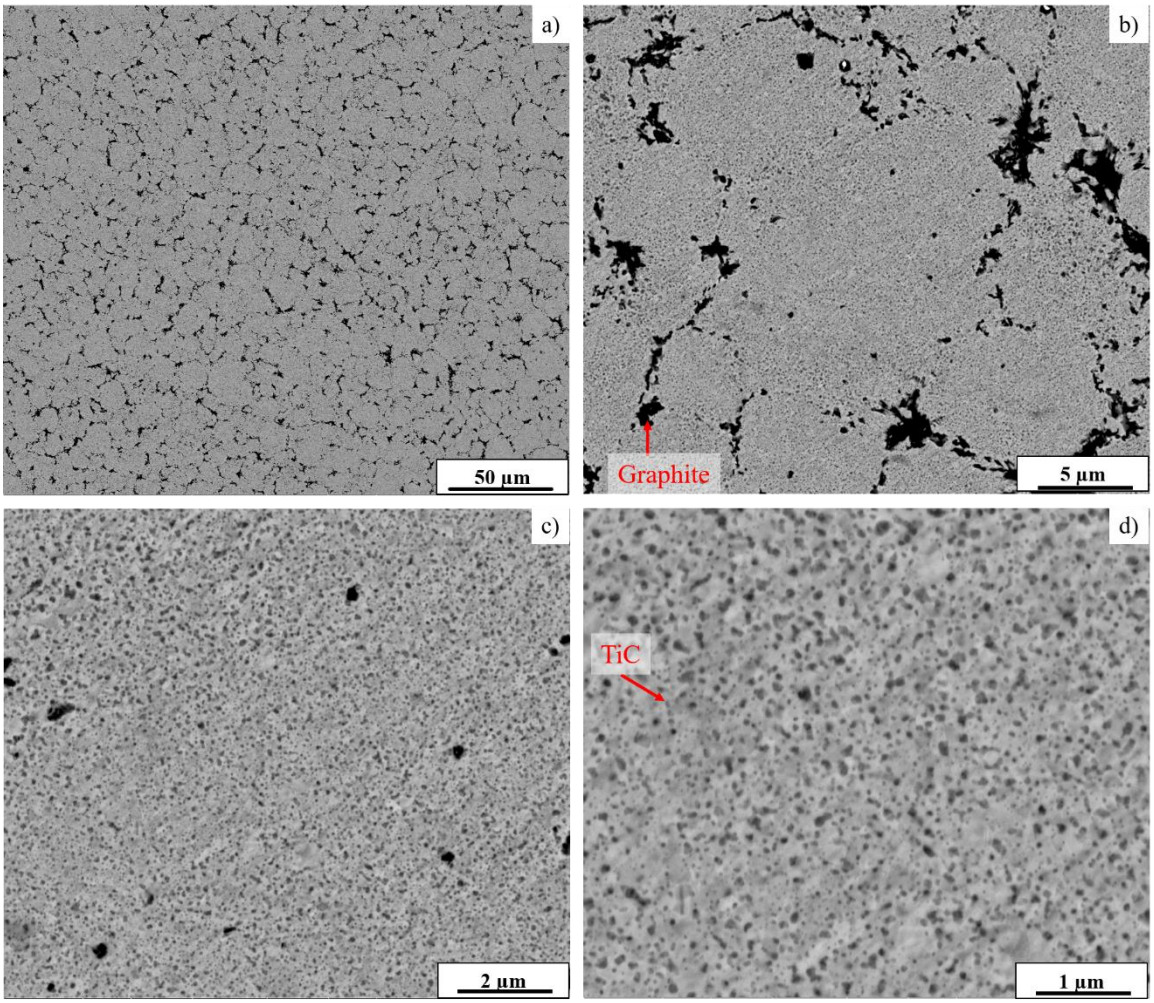

Figure 8: Backscattered images of Ni-10Ti-10C at a) 1KX, b) 10 KX, c) 25KX, d) 50KX magnification

Figure 8 shows that Ni-10Ti-10C exhibits, uniform dispersion of TiC precipitates within nickel matrix. Also, in SPS processed Ni-10Ti-10C sample, some unreacted graphite was observed indicating that not all the titanium reacted with graphite for *in situ* TiC formation, and maybe solid solution with nickel matrix is formed even though carbon has negligible solubility with pure nickel. High volume fraction of homogeneously distributed TiC precipitates is clearly seen in Figure 8. This was expected due to high content (at%) of titanium and carbon as compared to Ni-10Ti-5C, which promotes *in situ* TiC formation during mechanical alloying followed by SPS processing. Moreover, it was also seen that due to higher C/Ti atomic ratio in Ni-10Ti-10C composites, the size as well

as volume fraction of TiC precipitates are larger as compared to Ni-10Ti-5C composites still retaining their spherical morphology.

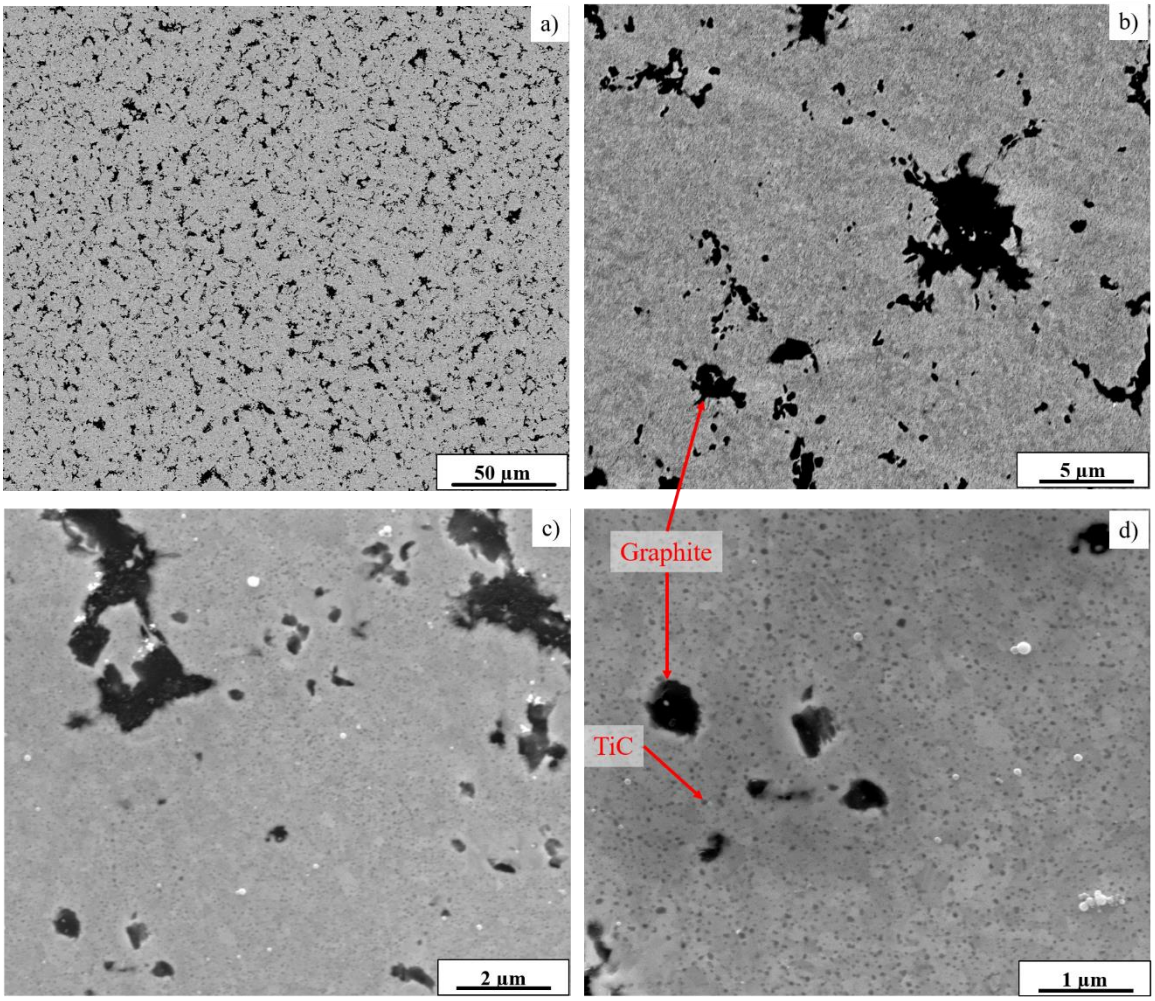

Figure 9: Backscattered images of Ni-5Ti-10C at a) 1KX, b) 10 KX, c) 25KX, d) 50KX magnification

Figure 9. shows SEM images of Ni-5Ti-10C composites. The presence of extra graphite phase exhibiting acicular morphology left after the reaction of titanium with carbon forming *in situ* TiC precipitates has been clearly seen. From Figure 9. it can be clearly seen that the volume fraction and size of TiC precipitates present in Ni-5Ti-10C are smaller as compared with Ni-10Ti-10C composite since lower (at%) of titanium were available to form *in situ* TiC precipitates.

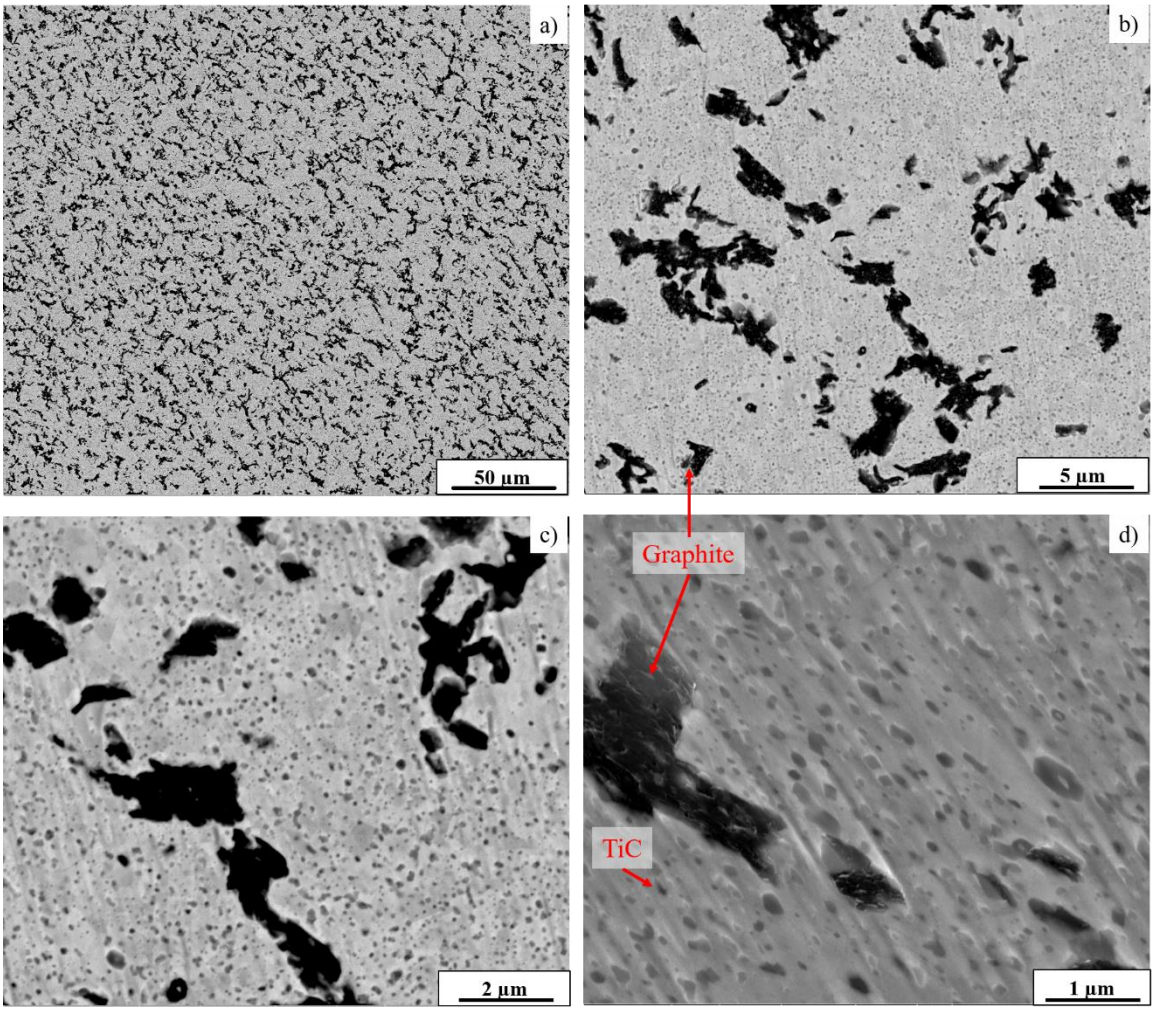

Figure 10: Backscattered images of Ni-7Ti-20C at a) 1KX, b) 10 KX, c) 25KX, d) 50KX magnification

SEM images of Ni-7Ti-20C are shown in Figure 10. It clearly shows homogeneous distribution of *in situ* TiC precipitates within the nickel grains along with present of extra graphite phase in the nickel matrix. In comparison with Ni-5Ti-10C the volume fraction of *in situ* TiC precipitates and graphite phase present in Ni-7Ti-20C are more, also coarser TiC precipitates have been observed as compared to Ni-5Ti-10C composites. This is mainly attributed to the increased content of both titanium and carbon in the composite.

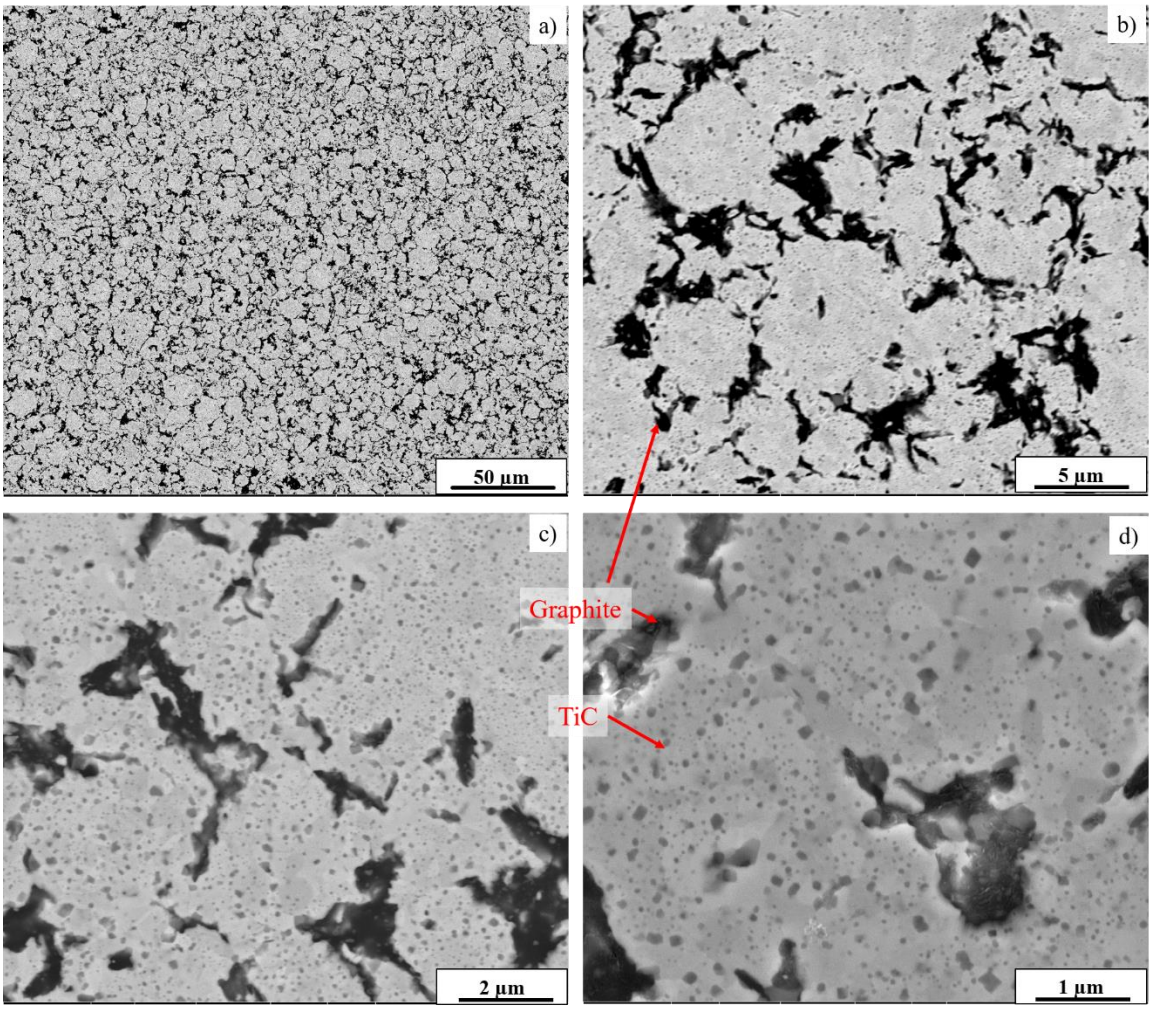

Figure 11: Backscattered images of Ni-6Ti-20C at a) 1KX, b) 10 KX, c) 25KX, d) 50KX magnification

Figure 11. shows backscattered images of Ni-6Ti-20C. It shows increment in volume fraction of graphite phase and decrease in TiC precipitates as compared with Ni-7Ti-20C, which was expected. Also, bimodal size distribution of *in situ* TiC precipitates has been clearly seen in Ni-6Ti-20C composites, which required further investigation.

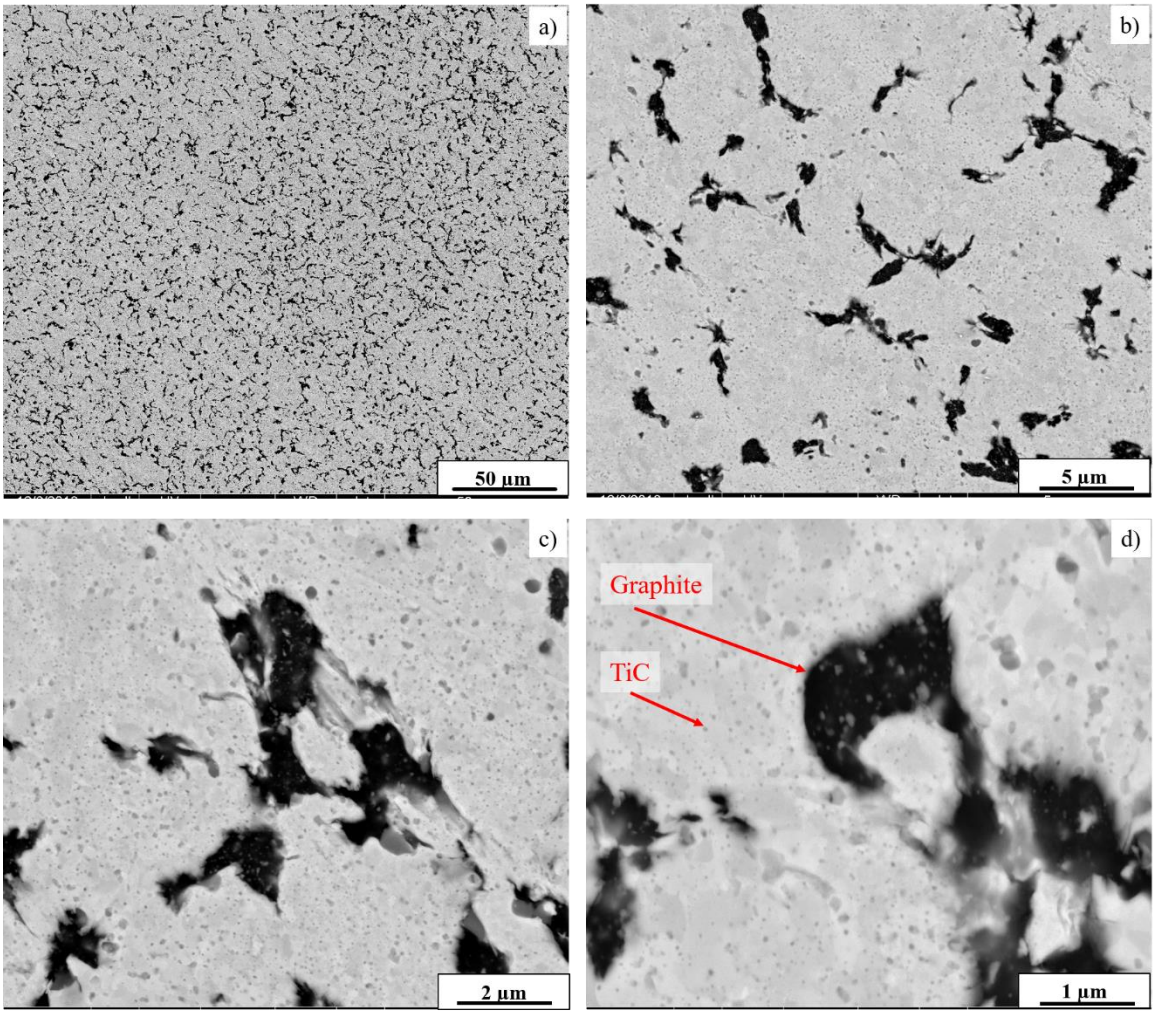

Figure 12: Backscattered images of Ni-5Ti-20C at a) 1KX, b) 10 KX, c) 25KX, d) 50KX magnification

Figure 12. shows SEM images of SPS processed Ni-5Ti-20C composite. In this micrograph it can be observed that the volume fraction of TiC precipitates is lower as compared to Ni-10Ti-10C, Ni-7Ti-20C, and Ni-6Ti-20C. Also, coarser and uniformly distributed graphite phase within nickel matrix has been clearly seen primarily due to higher atomic percent of graphite present in these composites.

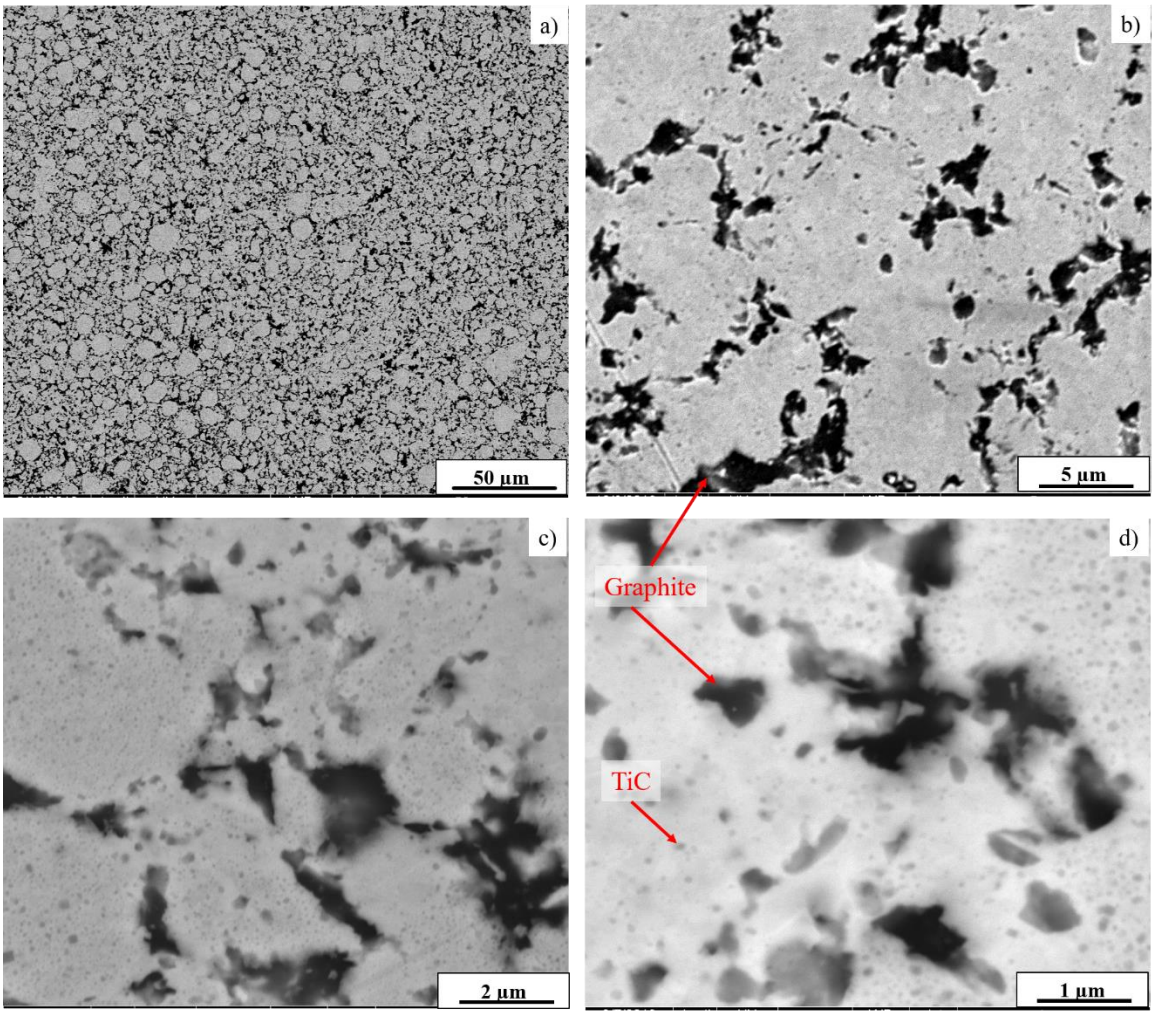

Figure 13: Backscattered images of Ni-4Ti-20C at a) 1KX, b) 10 KX, c) 25KX, d) 50KX magnification

Figure 13. shows SEM images of SPS processed Ni-4Ti-20C composite. It shows increased volume fraction of graphite phase with decrease in TiC precipitates as compared to Ni-7Ti-20C and Ni-6Ti-20C. It can be clearly seen from the micrographs that as the C/Ti ratio increases, the volume fraction of graphite phase is these composites increases.

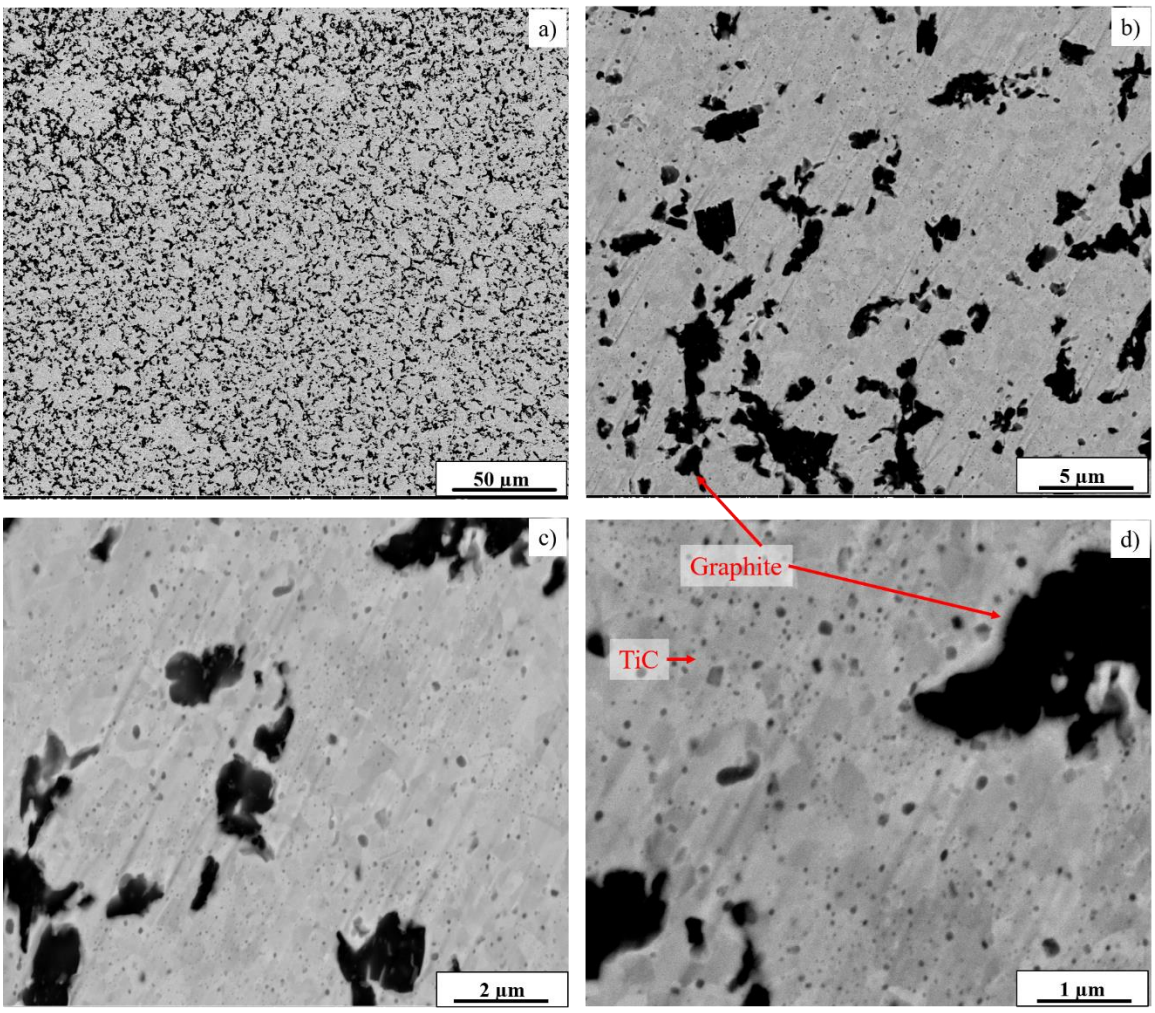

Figure 14: Backscattered images of Ni-3Ti-20C at a) 1KX, b) 10 KX, c) 25KX, d) 50KX magnification

Micrographs of Ni-3Ti-20C composites are shown in Figure 14. As compared to previous Ni-Ti-C composites lowest volume fraction of TiC precipitates were observed in these Ni-3Ti-20C composites, due to presence of very less at% of titanium available to react with graphite in order to form *in situ* TiC precipitates. It is apparent that, the volume fraction of *in situ* TiC precipitates decreases and volume fraction of graphite phase in Ni-Ti-C composites increases as the C/Ti ratio increases.

This microstructural characterization shows that pure nickel exhibits coarser grains as compared to that of Ni-Ti-C composites, as no second phase precipitates such as TiC

and graphite are present to restrict the grain boundaries and limit the grain growth during sintering. Backscattered micrographs of Ni-Ti-C composites clearly indicate that the dimension of *in situ* formed spherical TiC precipitates are in nanosized level and are uniformly dispersed in the nickel matrix. Crystallite size of TiC precipitates in Ni matrix remained in nanosized even after SPS processing. The TiC precipitates bordering graphite phase has also been observed since *in situ* TiC forms near graphite source due to availability of carbon in the composition. Additionally, acicular graphite region is also visible and uniformly distributed within nickel matrix. This is mainly due to unreacted carbon/graphite left after *in situ* TiC formation, exhibiting extra/unreacted graphite phase available in the matrix, which increases the wear resistance of the composite due to inherent solid lubrication nature of graphite, making it suitable for high temperature surface engineering application. Also, randomly oriented nickel grains have been observed in all Ni-Ti-C composites validating the feasibility of mechanical alloying and spark plasma sintering techniques for processing these *in situ* metal matrix composites.

4.1.3. Vickers microhardness

Vickers microhardness of SPS processed Ni-Ti-C composites is shown in Figure 15. It is observed that the microhardness drastically increased due to addition of titanium carbide reinforcement in nickel matrix as compared with pure nickel depicting hardness value of 147 VHN. It can be attributed to the clean interfacial bond, refined size, uniformity, and interfacial strength of *in situ* formed TiC particulates.

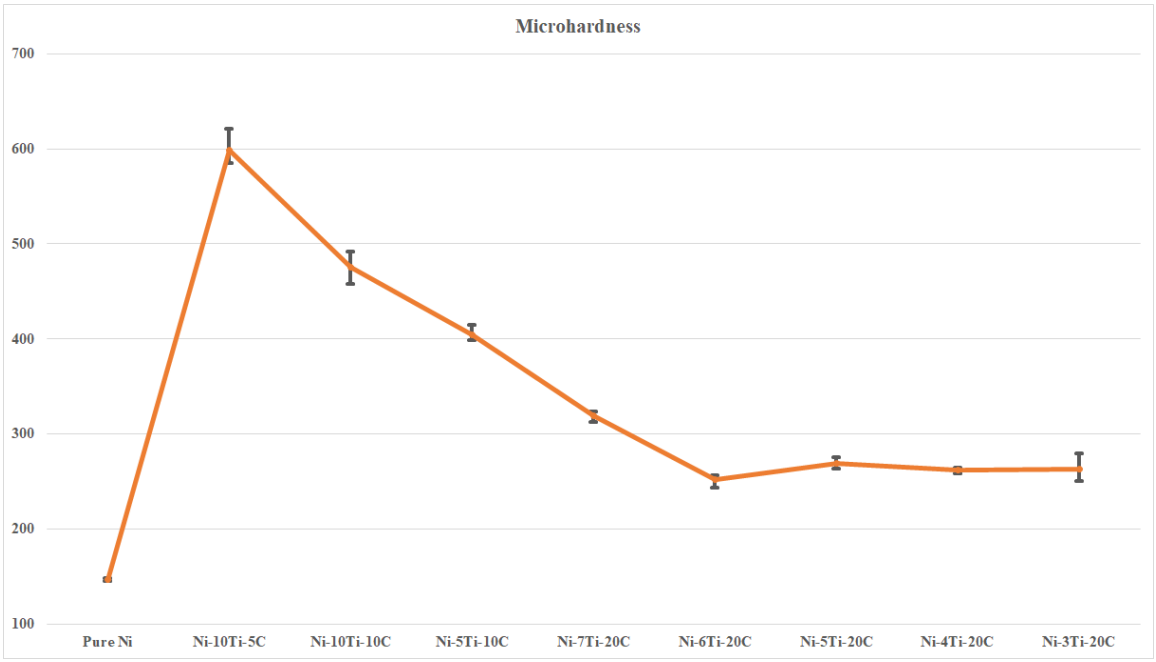

Figure 15: Vickers microhardness of SPS processed samples

Ni-10Ti-5C exhibited the highest hardness value of 598 VHN. composite, this can be attributed to presence is mainly due to high volume fraction of TiC reinforcement present and excess of Titanium in the Nickel matrix. Highest microhardness was expected in Ni-10Ti-10C as compared to Ni-10Ti-5C, however it exhibited hardness value of 475 VHN which is lower as compared with Ni-10Ti-5C. It may be due to presence of unreacted graphite which is also seen in the backscattered micrograph of Ni-10Ti-10C.

From Figure 15. it is apparent that the microhardness decreases as C/Ti ratio increases, which was expected and can be attributed to reduction in the volume fraction of TiC precipitates and increase in volume fraction of graphite phase in the composite. Ni-7Ti-20C exhibited hardness value of 318 VHN. However, as the C/Ti ratio increased further not much variation in microhardness value was observed. This is due to reduction of titanium content in the composition, resulting in very less *in situ* TiC formation along with presence of lubricious graphite phase dispersed throughout the sample.

An increase in microhardness clearly indicates pronounced improvement in the mechanical performance of the composite. This is mainly due to dispersion strengthening, smaller grain size, and grain boundary strengthening.

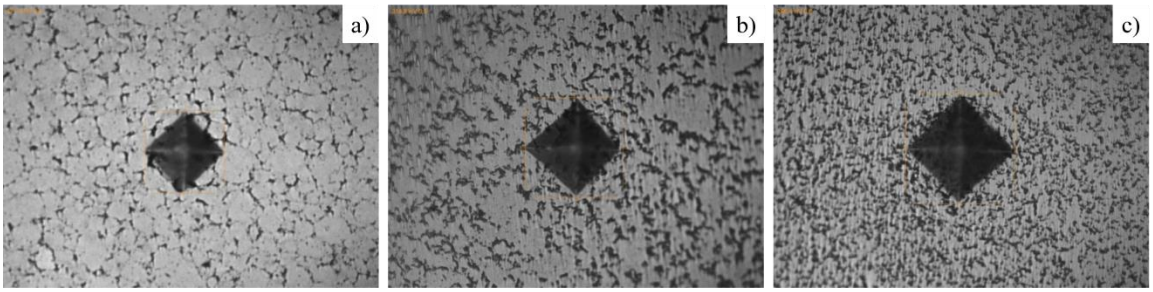

Figure 16: Vickers indent impression on a) Ni-10Ti-10C, b) Ni-7Ti-20C, c) Ni-3Ti-20C

Figure 16. shows indent impression of Vickers pyramid on the sample used for the measurement of the Vickers hardness number. The images were taken at 50X magnification. Indent on Ni-10Ti-10C has an average diagonal of ~45µm. The average diagonal size of indent impression on Ni-7Ti-20C was measured as ~54µm. It can be attributed to presence of hard carbide precipitates present in the sample, acting as a barrier for indent penetration. The diagonal size of indent impression in graphite rich Ni-3Ti-20C was found to be ~60µm. This trend clearly indicates that the diagonal size of indent was found to be increased C/Ti ratio was increased, which resulted in decrease hardness number. It is observed that microhardness decreases with increase in volume fraction of soft graphite phase present in the composites. A literature study reveals that this decrease in microhardness is due to graphite agglomeration.[22] However, despite large volume fraction of graphite phase in Ni-3Ti-20C composite, it still exhibited relatively higher microhardness or almost twice as that of pure nickel.

4.1.4. Tribological test

Ball on disc tribometry tests were performed under a normal load of 100g (1 N) using a 0.125" Si_3N_4 ball. Tests were carried out with track radius of ~2.5 mm and at constant sliding speed of 2.0-2.1 cm/sec. Steady-state friction behavior was observed and coefficient of friction (CoF) was calculated for a sliding distance of 140m for SPS processed Ni-10Ti-10C, Ni-5Ti-10C, Ni-7Ti-20C, and Ni-3Ti-20C samples.

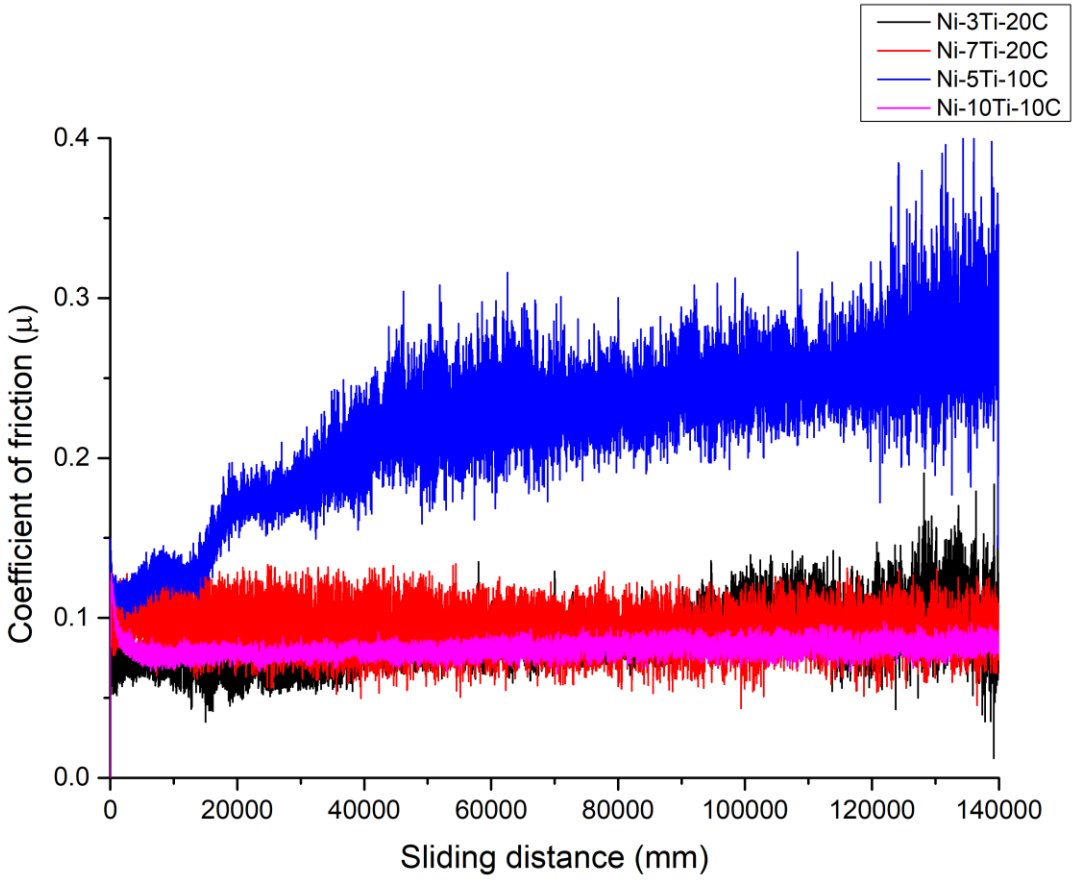

Figure 17: Steady state friction of SPS processed samples

Figure 17. shows steady state coefficient of friction (CoF) for SPS processed Ni-Ti-C composites. Lowest coefficient of friction value of ~0.08 was obtained for Ni-3Ti-20C. Second lowest CoF value was seen for Ni-10Ti-10C, which was unexpected. But this resulted mainly due to presence of unreacted graphite phase present in the composite along

with TiC precipitates, both beneficial in forming a good lubricious tribofilm on the surface. Average coefficient of friction value of ~0.09 was seen for Ni-7Ti-20C, which was expected due to presence of lubricious graphite phase in the composite is beneficial in reducing the coefficient of friction.

Highest coefficient of friction value of ~0.2 was obtained for Ni-5Ti-10C in comparison with other samples. This is attributed to low volume fraction of graphite present in the sample, which is also apparent from the SEM micrographs. Also, it was observed that coefficient of friction increased at a constant rate over time, exhibiting non steady state behavior. It may be due to poor adhesion between the phases or large distance between the graphite phases which prevents the formation of tribofilm on surface of the sample. Another reason for this unusual behavior can be caused due to severity in the movement of the pin over wear debris deposited on the sliding track from previous run leading to asperity on the surface. This causes abrupt increase in temperature at the contact area which favors the adhesive phenomena, thus increases the coefficient of friction.[56]

4.2. LENS™ processed Ni-Ti-C composites

4.2.1. X-Ray diffraction analysis

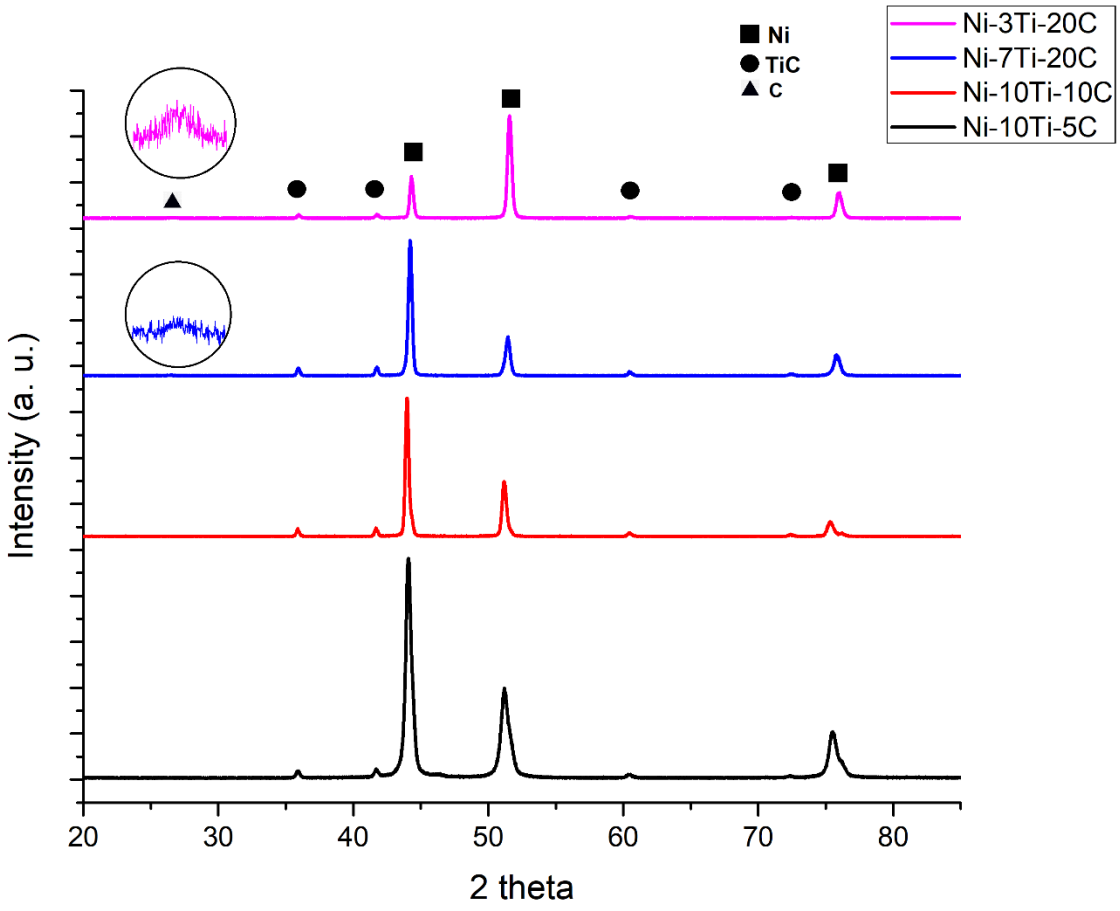

Figure 18: XRD pattern for LENS™ processed samples

Figure 18. shows the x-ray diffraction patterns for LENS™ processed Ni-Ti-C. Ni-10Ti-5C and Ni-10Ti-10C exhibited FCC nickel as well as FCC titanium carbide (TiC) phases without presence of any HCP graphite peak. This clearly shows that titanium and graphite has undergone *in situ* reaction during LENS™ processing forming titanium carbide (TiC). Peaks corresponding (111), (200), and (220) crystallographic planes of FCC nickel, whereas peaks corresponding (111), (200), (220) and (311) crystallographic planes

of FCC titanium carbide phase were observed at the position which agrees with the X-ray diffraction data files of pure nickel and TiC.[58] Increase in peak intensity of FCC titanium carbide was observed mainly due to increase in the volume fraction of TiC precipitates which will be shown in microstructural analysis. No intermetallic phases such as NiTi, Ni_3C were observed. Additionally, peak corresponding to graphite phase is shown in enlarged view, as it reflected relatively low intensity as compared to other phases. No peak corresponding to graphite phase was observed in Ni-10Ti-5C and Ni-10Ti-10C, this indicates that all the carbon present in the composition undergone *in situ* reaction with titanium forming TiC precipitates. The HCP (0002) peak reflecting at ~26^0 was seen only in Ni-7Ti-20C and Ni-3Ti-20C, which was expected due to excess amount of carbon. Also, there is an increase in intensity of (0002) carbon peak as the C/Ti ratio increases.

4.2.2. Microstructural analysis

SEM images of Ni-10Ti-5C and NI-10Ti-10C is shown in Figure 19. From the micrograph it is clearly visible that titanium and carbon has undergone *in situ* reaction forming TiC precipitates in the nickel matrix. This uniform distribution of the TiC precipitates can be attributed to the stirring effect produced by the high energy density beam. Vigorous convection flow due to motion of liquid metal in the melt pool is another reason for homogeneous distribution of the *in situ* formed reinforcement precipitates throughout the microstructure.[43,55]

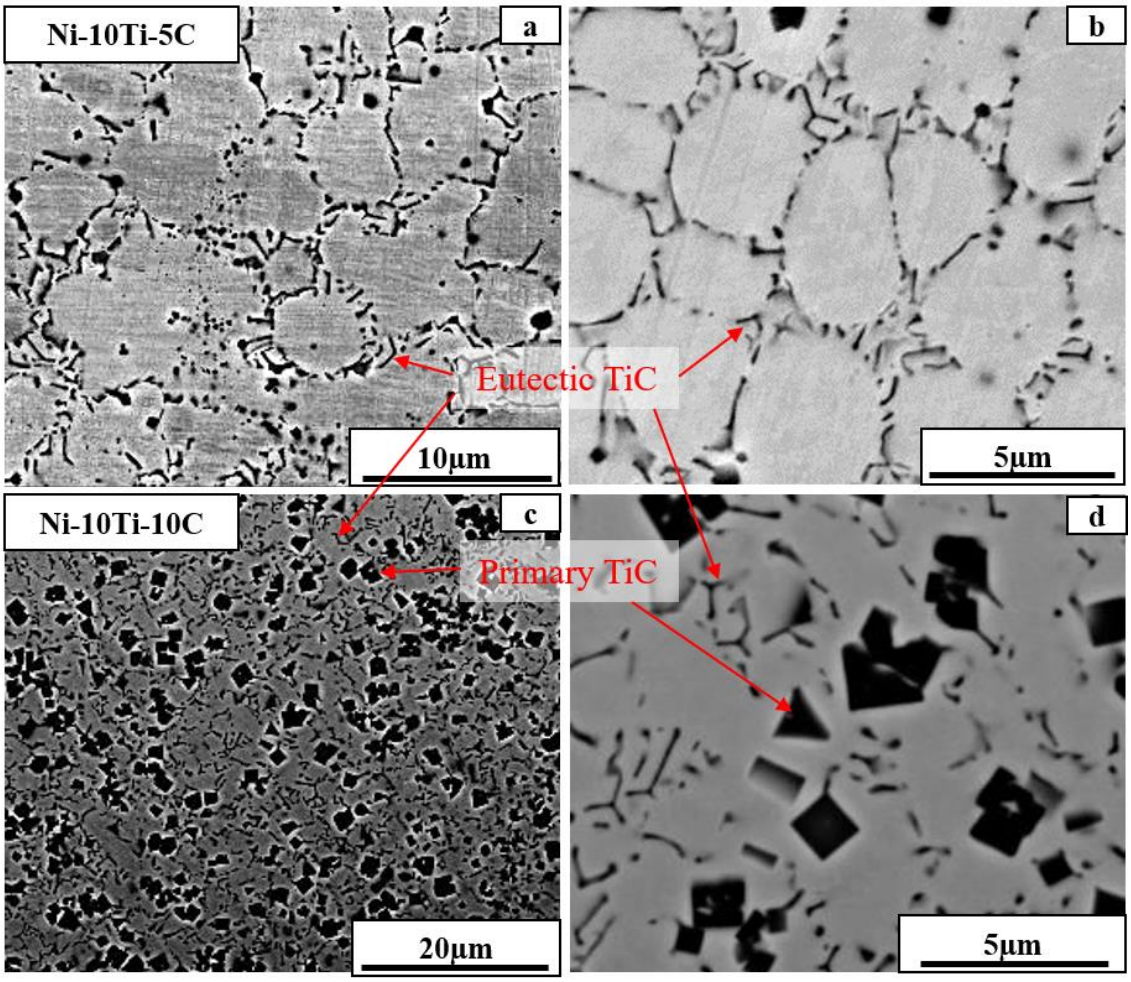

Figure 19: Backscattered images of LENS^{TM} processed sample a) Ni-10Ti-5C @ 5KX b) Ni-10Ti-5C @ 20KX c) Ni-10Ti-10C @ 2KX d) Ni-10Ti-10C @ 20KX

Ni-10Ti-5C composite exhibits presence of needle shape TiC precipitates uniformly distributed in the nickel matrix. These observed TiC precipitates are primarily eutectic TiC precipitates obtained during solidification of molten Ni-10Ti-5C composites. Ni-10Ti-10C composite exhibits cuboidal as well as needle shape TiC. Micron sized cuboidal TiC are primary TiC, whereas fine scaled needle shape TiC are eutectic TiC. In this Ni-10Ti-10C composites, primary TiC acts as a heterogeneous nucleation sites for eutectic TiC during solidification.[7] Volume fraction of TiC precipitates is more in Ni-10Ti-10C as compared to Ni-10Ti-5C composites, due to higher at% of carbon present for titanium to react forming *in situ* TiC precipitates. A pseudo binary section of ternary Ni-Ti-C system is shown Figure 20.

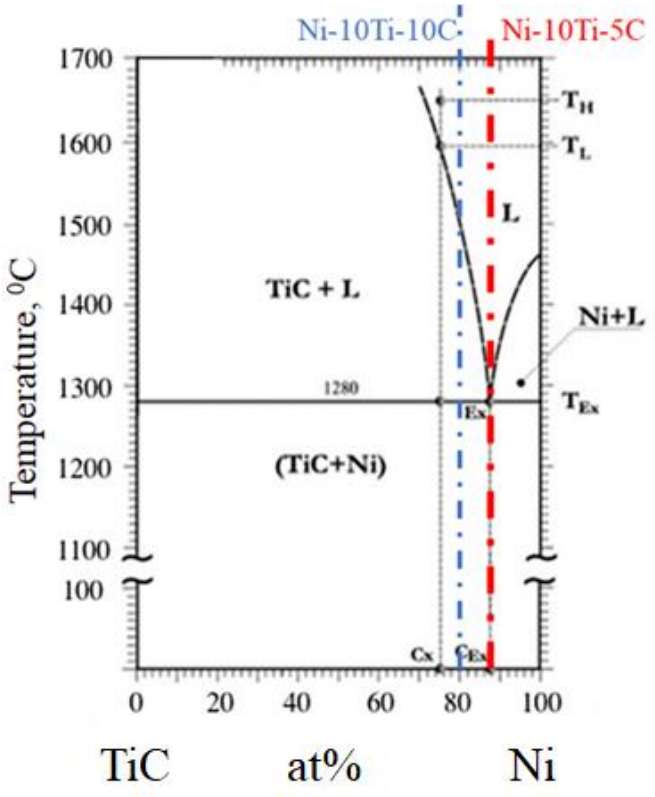

Figure 20: Pseudo binary section of ternary Ni-Ti-C system[57]

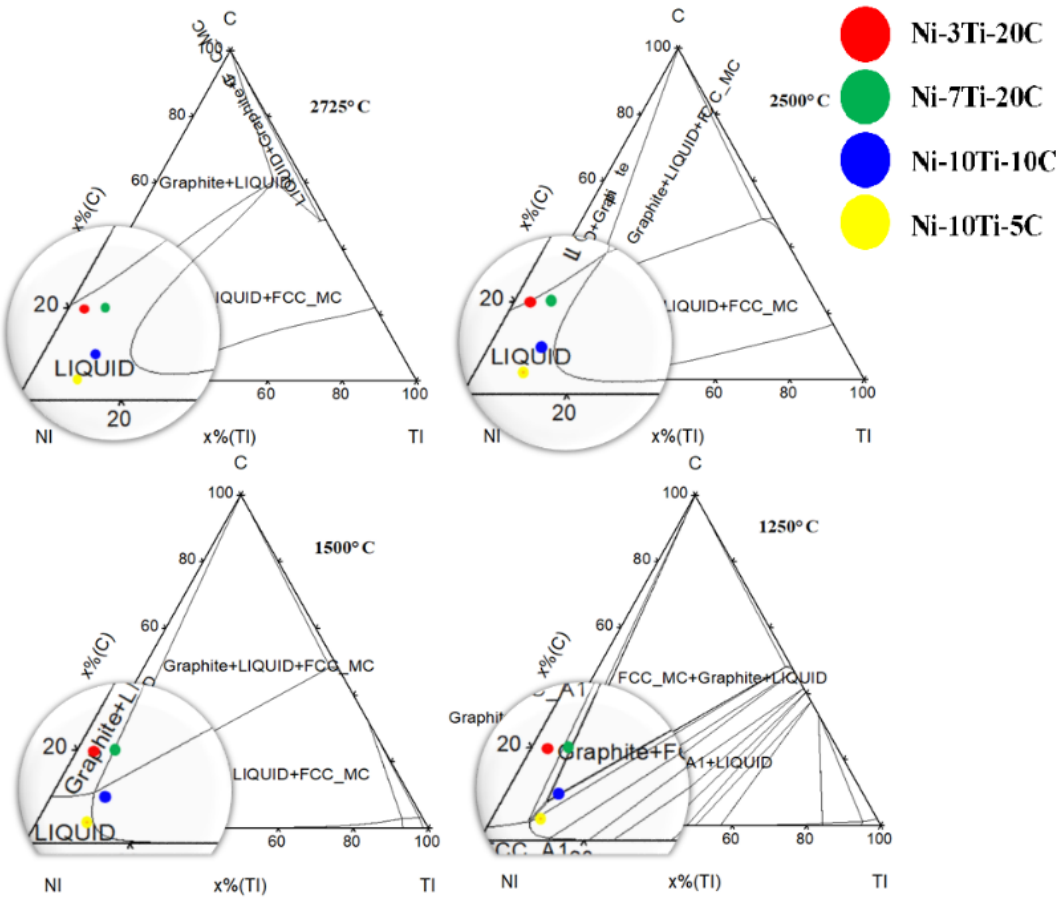

Figure 21: Ternary phase diagram of Ni-Ti-C system

Figure 21. shows ternary phase diagram of Ni-Ti-C system. It is shown that at temperature of 2725^0C both nickel and *in situ* formed TiC are in liquid phase. During cooling as the temperature falls below 2500^0C primary TiC starts forming in the melt pool. As the temperature falls further below 1280^0C, the remaining liquid in the melt pool undergoes pseudo-binary solidification forming eutectic Ni and eutectic TiC. It can be observed from the SEM images that the primary TiC acts as a nucleation site for the formation of eutectic TiC. In case of Ni-10Ti-5C where the nickel content is 85%, phase evolution different than that of Ni-10Ti-10C was observed. In Ni-10Ti-5C only eutectic TiC was formed on solidification. The pseudo-binary isothermal section of Ni-Ti-C system shown in Figure 21. helps to understand phase transformation in these Ni-Ti-C composites.

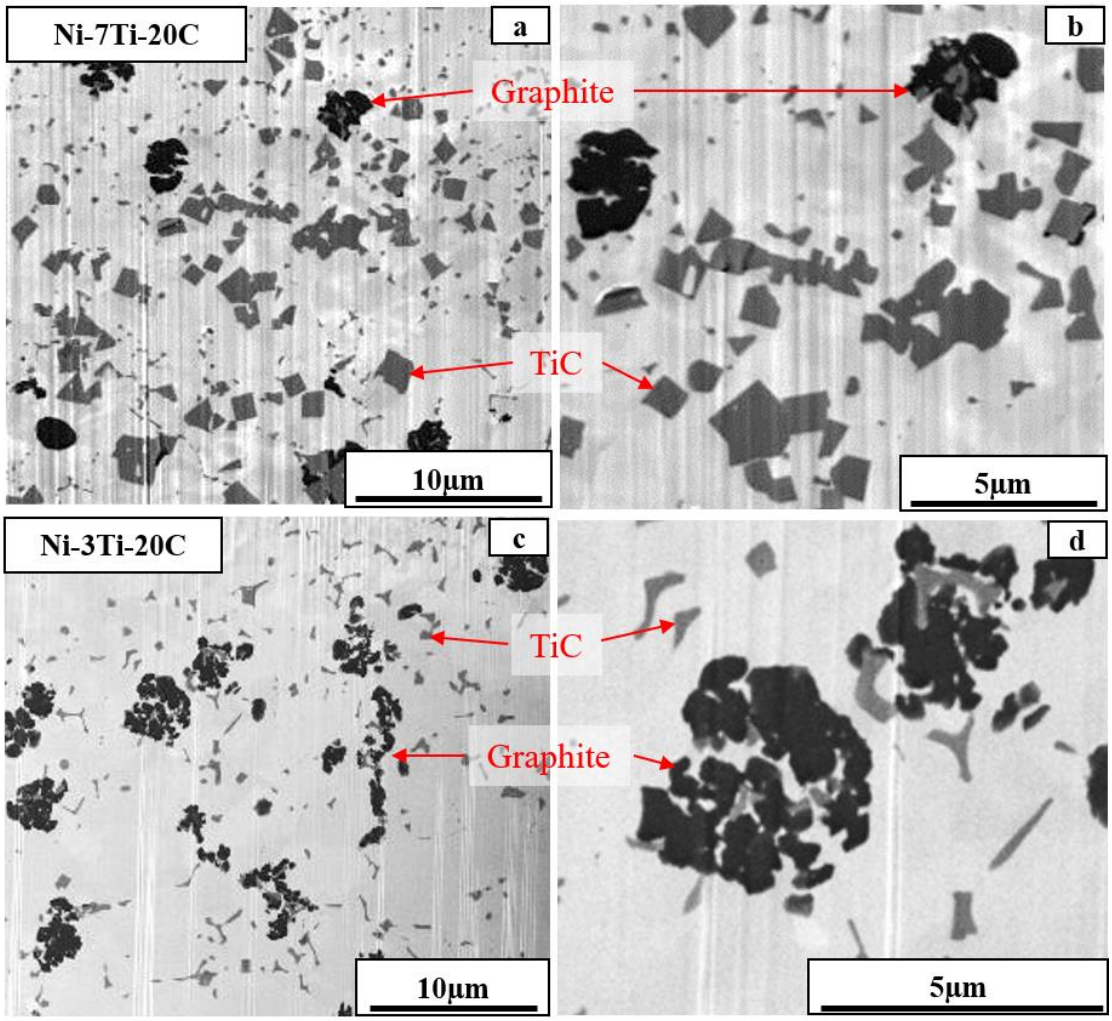

Figure 22: Backscattered images of LENS^{TM} processed sample a) Ni-7Ti-20C @ 5KX b) Ni-7Ti-20C @ 20KX c) Ni-3Ti-20C @ 5KX d) Ni-3Ti-20C @ 30KX

Figure 22. shows backscattered images of Ni-7Ti-20C and Ni-3Ti-20C. In Ni-7Ti-20C and Ni-3Ti-20C both primary TiC as well as eutectic TiC were observed within the nickel matrix. It can also be seen that higher volume fraction as well as coarser titanium carbide precipitates have been observed in Ni-7Ti-20C as compared to Ni-3Ti-20C composites primarily due to high at% of titanium present for *in situ* chemical reaction.

Additionally, graphite phase with acicular morphology was also visible in Ni-7Ti-20C and Ni-3Ti-20C micrographs. High volume fraction of graphite phase has been

observed in Ni-3Ti-20C, which is mainly due to low at% of titanium available to react with carbon. These observations are consistent with what we have seen in x-ray diffraction analysis. This increased volume fraction of Graphite plays an important role considerably reducing the coefficient of friction. Also, it was observed that volume fraction and size of primary TiC are lower in Ni-3Ti-20C as compared to Ni-7Ti-20C.

4.2.3. Vickers microhardness

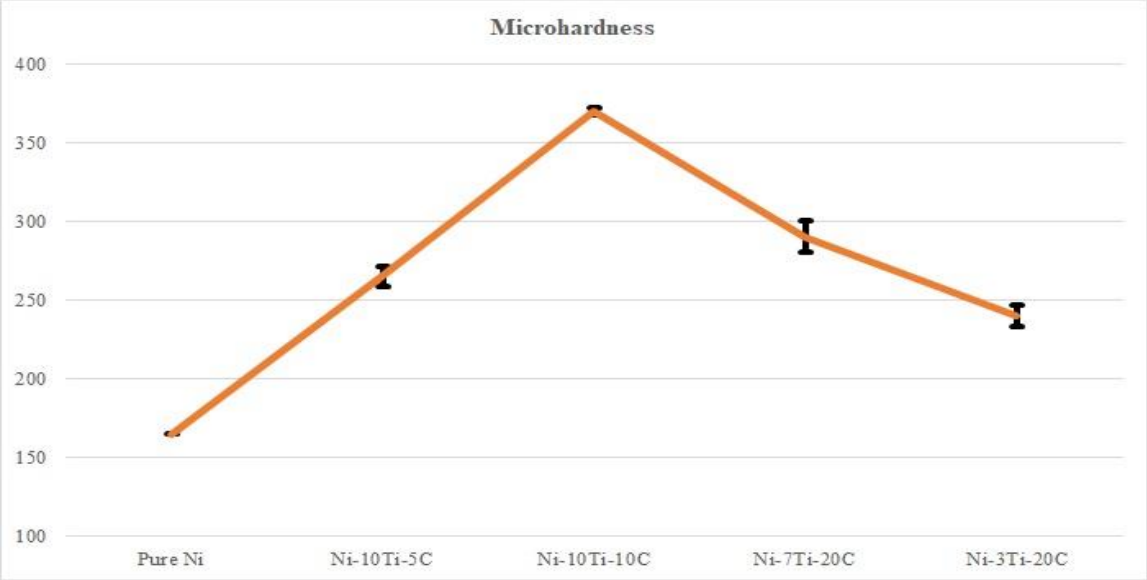

Figure 23: Vickers microhardness of LENS^{TM} processed samples.

Figure 23. clearly indicates change in the microhardness number, as the function of increasing C/Ti ratio. The highest microhardness was recorded for Ni-10Ti-10C, its mainly due to high volume fraction of *in situ* formed primary as well as eutectic TiC precipitates. This *in situ* formed homogeneously dispersed TiC precipitates acts as a barrier for grain boundary dislocation, therefore the penetration of indent is restricted. Ni-7Ti-20C and Ni-3Ti-20C exhibit lower microhardness value than Ni-10Ti-10C due to lower volume fraction of hard TiC precipitates and higher volume fraction of soft graphite phase present.

Also, as expected the hardness number for the composite decreased as the C/Ti ratio increased. This can be attributed to reduction in TiC precipitate, and an increase in graphite content in the composite. Moreover, standard deviation represented in error bar also shows that the readings were consistent throughout the sample. This very small variation in obtained microhardness number clearly indicates the homogeneous dispersion of TiC phase and graphite phase in the sample, which was also noticed from backscattered micrographs of the sample.

4.2.4. Tribological test

Tribological test were performed under a normal load of 100g (1 N) using a Si_3N_4 ball. Test was carried out with track radius of ~2.14 mm and at constant sliding speed of 2.1-2.2 cm/sec. Steady-state friction behavior was observed and coefficient of friction (CoF) was calculated for a sliding distance of 140m for LENS^{TM} deposited pure Ni, Ni-10Ti-10C, Ni-10Ti-5C, Ni-7Ti-20C, and Ni-3Ti-20C samples.

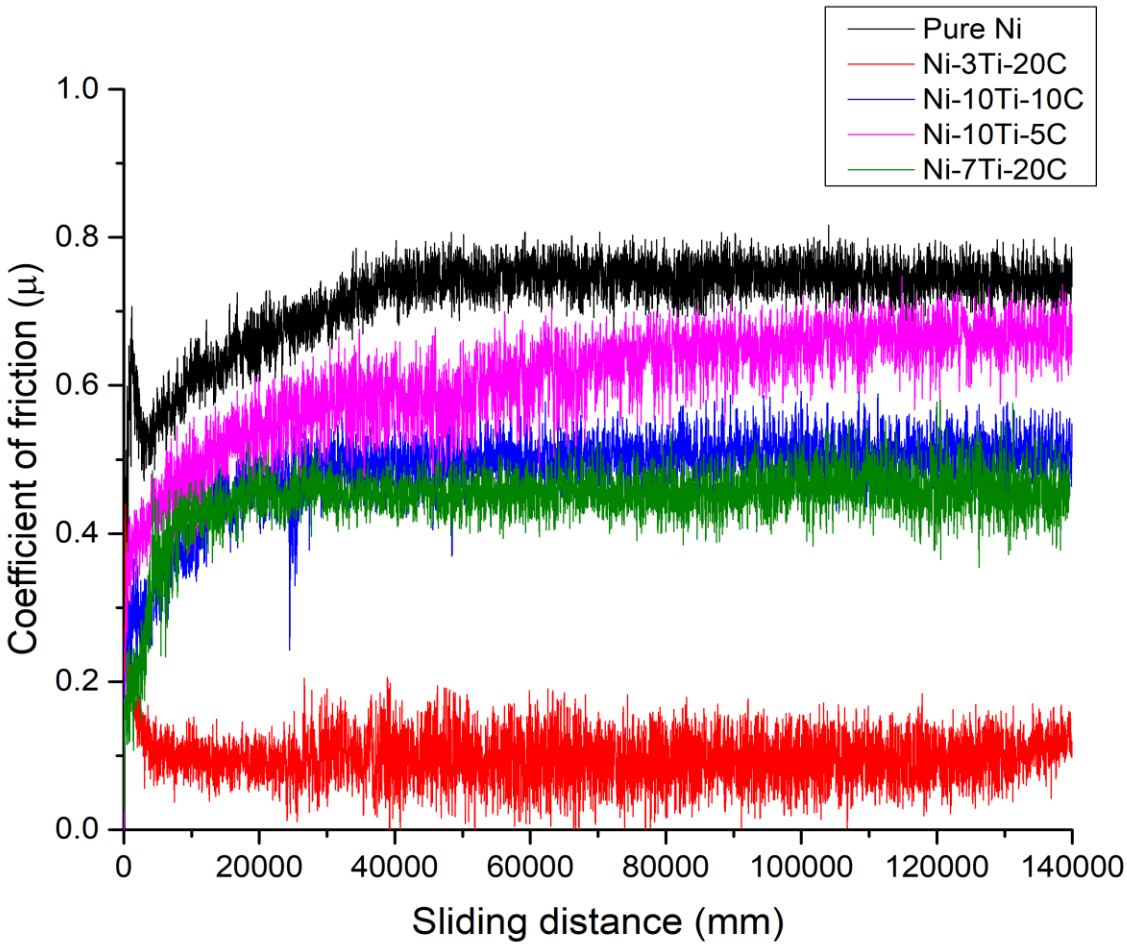

Figure 24: Steady state friction of LENS^{TM} processed samples

Figure 24. shows steady state coefficient of friction for LENS^{TM} processed Ni-Ti-C composites. Pure nickel exhibited highest coefficient of friction of ~0.7 as compared with Ni-TiC-C composites. It was obvious as metallic nickel exhibits adhesive behavior and has no lubricious friction properties. Lowest value of CoF value of ~0.1 was obtained for Ni-3Ti-20C, which is mainly due to high volume fraction of graphite phase present in the composition. Later, it was observed, that the coefficient of friction value increased as the volume fraction of lubricious graphite present in the sample was reduced.

4.2.5 EDS mapping

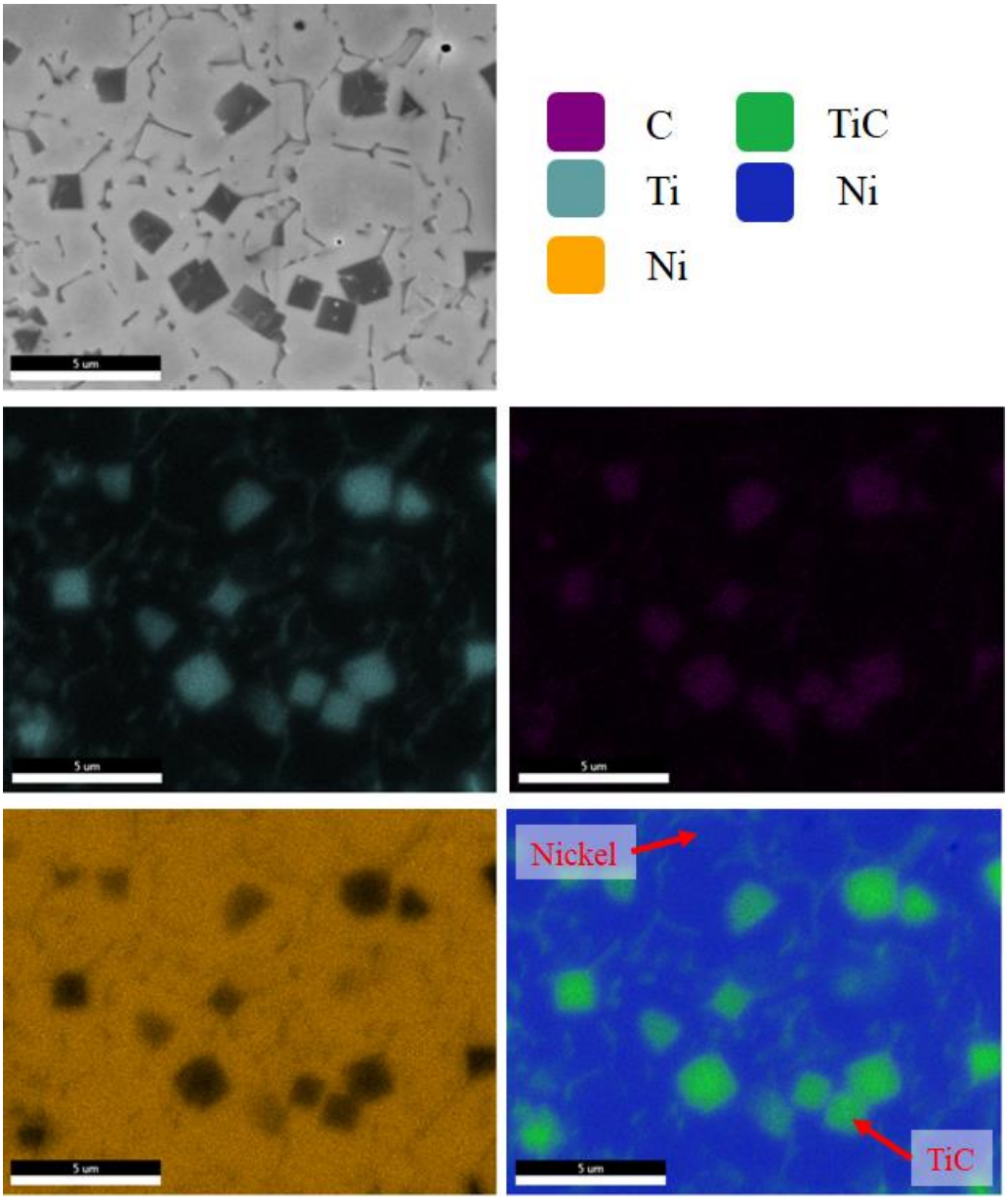

Figure 25: EDS maps of Ni-10Ti-10C

Figure 25. shows SEM image of LENS^{TM} processed Ni-10Ti-10C its EDS maps of C, TiC, and Ni. The EDS maps reveal the dispersion of TiC precipitates within the nickel matrix and is in congruence with the XRD and SEM results. It indicates the presence of primary TiC and eutectic TiC in the nickel matrix.

4.3. SPS process vs LENS^{TM} process

Figure 26: Microhardness comparison between SPS and LENS^{TM} processed samples

Figure 26. shows difference in microhardness of composites of same nominal compositions but fabricated using two different processing techniques, one using MA followed by SPS process and other using LENS^{TM} process.

In processing using MA followed by SPS technique, *in situ* TiC precipitates are formed due to solid-solid reaction process. In this process it was observed that nanosized TiC precipitates are formed due to exothermic reaction during MA. Later, the fabrication was carried out using SPS technique which allowed sintering at relatively lower temperature below the melting point with shorter sintering time. In this process fabrication is carried out via solid state reaction which retards the grain growth of nickel. Whereas, in LENS^{TM} process the *in situ* reaction take place via solid-liquid reaction. In this reaction, a melt pool

is formed at a temperature relatively higher as compared to SPS processing, thus the grain sizes of nickel as well as *in situ* formed TiC precipitates are larger. This increased size of TiC precipitates and nickel grain reduces the hardness of the composites as compared to SPS processed Ni-Ti-C composites.

It is clearly seen that the composites fabricated using MA and SPS process possess higher hardness as compared to LENS^{TM} deposited composites. It can be attributed mainly to the large volume fraction of nanosized and more uniform dispersion of *in situ* formed TiC precipitates within the nickel matrix. The reinforcement precipitates formed in LENS^{TM} processed composite is also uniformly distributed but are coarser as compared to former process which has also seen in SEM micrographs. It clearly indicates that, the formation of nanosized *in situ* reinforcement via MA and the restricted grain growth in SPS process leads to the high microhardness of the composite.

CHAPTER V

CONCLUSION

Fabrication of *in situ* TiC/C precipitates reinforced in nickel matrix was carried out successfully using powder metallurgy route by mechanically alloying followed by spark plasma sintering process and, by metal additive manufacturing technique, i.e. LENS^{TM} processing technique.

Microstructure evolution and mechanical properties of the processed composites were investigated successfully via SEM, XRD, Vickers hardness test, and tribological test. The results indicate that *in situ* TiC reinforcement in the nickel matrix substantially increases the hardness of the materials. By altering C/Ti ratio, change in the volume fraction as well as size of TiC precipitates has been attained and was also able to engineer an extra graphite phase in these composites, which considerably lowered the coefficient of friction as compared with pure nickel.

Homogeneous distribution of *in situ* reinforcement has been achieved using both the processing routes. In Ni-TiC composites processed via MA followed by SPS technique, it was observed that the dispersion of *in situ* formed TiC precipitates within the nickel matrix was homogeneous and were in nanosized with spherical morphology. It is mainly

attributed to mechanical alloying via high energy ball milling followed by spark plasma sintering. Whereas, two different morphologies of TiC precipitates with size ranging in few microns have been observed in LENS^{TM} processed composites. The cuboidal shaped primary TiC acting as a heterogeneous nucleation site for the precipitation of fine needle-shaped eutectic TiC precipitates during solidification of these Ni-Ti-C composites.

In Ni-Ti-C composites, it was observed that the hardness of the composite increases as the volume fraction of *in situ* TiC precipitates increases. The nanosized level of TiC precipitates attained via MA acts as a pinning point retarding grain growth. Also, the nickel grain size observed in SPS processed composites was much refined as compared to LENS^{TM} processed composites. This is mainly due to relatively low processing temperature and shorter holding time involved in SPS processing technique as compared to LENS^{TM} processed samples. Therefore, due to a relatively smaller size and more uniform dispersion of TiC precipitate within the nickel matrix, high microhardness was achieved in the SPS processed composites in comparison with LENS^{TM} processed counterparts.

Improvement in tribomechanical properties with a reduction in coefficient of friction was seen in Ni-Ti-C composites. It was seen that the coefficient of friction reduces as the C/Ti ratio increases. It can be attributed mainly due to increase in the volume fraction of lubricious graphite phase in these composites.

Therefore, the addition of hard TiC reinforcement and lubricious graphite phase in the nickel matrix increases hardness and reduces the coefficient of friction making it a suitable candidate for structural and surface engineering applications.

REFERENCES

1. Bakshi, Srinivasa R., Debrupa Lahiri, and Arvind Agarwal. "Carbon nanotube reinforced metal matrix composites-a review." *International materials reviews* 55.1 (2010): 41-64.
2. Ibrahim, I.A., Mohamed, F.A. & Lavernia, E.J. J Mater Sci (1991) 26: 1137-1156.
3. Miracle, D. B. "Metal matrix composites–from science to technological significance." *Composites science and technology* 65.15-16 (2005): 2526-2540.
4. Ye, L. L., and M. X. Quan. "Synthesis of nanocrystalline TiC powders by mechanical alloying." *Nanostructured materials*5.1 (1995): 25-31.
5. Zhu, Xinkun, *et al*. "Synthesis of nanocrystalline TiC powder by mechanical alloying." *Materials Science and Engineering: C* 16.1-2 (2001): 103-105.
6. Saheb, Nouari, *et al*. "Spark plasma sintering of metals and metal matrix nanocomposites: a review." *Journal of Nanomaterials* 2012 (2012): 18.
7. Borkar, Tushar, *et al*. "Laser-deposited *in situ* TiC-reinforced nickel matrix composites: 3D microstructure and tribological properties." *JOM* 66.6 (2014): 935-942.
8. Gopagoni, Sundeep, *et al*. "Microstructural evolution in laser deposited nickel–titanium–carbon *in situ* metal matrix composites." *Journal of Alloys and Compounds* 509.4 (2011): 1255-1260.
9. Wang, H., Zhang, S., Zhu, J., Huang, J., Liu, H., & Zhang, H. (2009). *In situ* TiC-Reinforced Ni-Based Composite Coating Prepared by Flame Spraying Using Sucrose as the Source of Carbon. *Journal of thermal spray technology*, *18*(1), 103-109.

10. Guo, Chun, *et al*. "Effects of WC–Ni content on microstructure and wear resistance of laser cladding Ni-based alloys coating." *Surface and Coatings Technology* 206.8-9 (2012): 2064-2071.
11. Choi, Chul-Jin. "Preparation of ultrafine TiC–Ni cermet powders by mechanical alloying." *Journal of Materials Processing Technology* 104.1-2 (2000): 127-132.
12. Tjong, S. C., and Z. Y. Ma. "Microstructural and mechanical characteristics of *in situ* metal matrix composites." *Materials Science and Engineering: R: Reports* 29.3-4 (2000): 49-113.
13. Suryanarayana, C. "Mechanical alloying and milling." *Progress in materials science* 46.1-2 (2001): 1-184.
14. Xiaobo, Zhou Jun Liu Ning Zhang, and Lu Maohua Rong Chunlan. "Effect of Particle Sizes on Microstructure and Mechanical Properties of Ti (C, N)-based Cermets [J]." *Cemented Carbide* 1 (2007).
15. Zheng, Yong, *et al*. "Effect of nano addition on the microstructures and mechanical properties of Ti (C, N)-based cermets." *Ceramics International* 31.1 (2005): 165-170.
16. Mamedov, V. "Spark plasma sintering as advanced PM sintering method." *Powder Metallurgy* 45.4 (2002): 322-328.
17. Viswanathan, Venkatachalapathy, *et al*. "Challenges and advances in nanocomposite processing techniques." *Materials Science and Engineering: R: Reports* 54.5-6 (2006): 121-285.

18. Borkar, Tushar, *et al*. "Strength versus ductility in carbon nanotube reinforced nickel matrix nanocomposites." *Journal of Materials Research* 29.6 (2014): 761-769.
19. Borkar, Tushar, and Rajarshi Banerjee. "Influence of spark plasma sintering (SPS) processing parameters on microstructure and mechanical properties of nickel." *Materials Science and Engineering: A* 618 (2014): 176-181.
20. Borkar, Tushar, *et al*. "Excellent strength–ductility combination in nickel-graphite nanoplatelet (GNP/Ni) nanocomposites." *Journal of Alloys and Compounds* 646 (2015): 135-144.
21. Munir, Zuhair A., Dat V. Quach, and Manshi Ohyanagi. "Electric current activation of sintering: a review of the pulsed electric current sintering process." *Journal of the American Ceramic Society* 94.1 (2011): 1-19.
22. Sharma, Pardeep, Satpal Sharma, and Dinesh Khanduja. "A study on microstructure of aluminium matrix composites." *Journal of Asian Ceramic Societies* 3.3 (2015): 240-244.
23. Gibson, Ian, David W. Rosen, and Brent Stucker. Additive manufacturing technologies. Vol. 17. New York: Springer, 2014.
24. Morris, David G. "Mechanical behavior of nanostructured materials." Materials science foundations 2 (1998): 26-84
25. Kaczmar, J., Pietrzak, K., & Wosiski, W. (2000). The production and application of metal matrix composite materials. Journal of Materials Processing Tech., 106(1 - 3), 58-67.

26. Pierson, Hugh O. Handbook of Refractory Carbides & Nitrides: Properties, Characteristics, Processing and Apps. William Andrew, 1996.
27. Zhuang, Jian, *et al*. "The influence of technological process on dry sliding wear behaviour of titanium carbide reinforcement copper matrix composites." Materials transactions 51.12 (2010): 2311-2317.
28. Upadhyaya, Gopal S. Powder metallurgy technology. Cambridge Int Science Publishing, 1997.
29. Angelo, P. C., and Ramayyar Subramanian. Powder metallurgy: science, technology and applications. PHI Learning Pvt. Ltd., 2008
30. Koch, C. C. "Intermetallic matrix composites prepared by mechanical alloying—a review." Materials Science and Engineering: A 244.1 (1998): 39-48.
31. Whittenberger, J. Daniel, Eduard Arzt, and Michael J. Luton. "Preliminary investigation of a NiAl composite prepared by cryomilling." Journal of Materials Research 5.2 (1990): 271-277.
32. Li, Yuxin, *et al*. "Effect of TiC content on Ni/TiC composites by direct laser fabrication." Materials & Design 30.4 (2009): 1409-1412.
33. Kumar, K. Ravi, K. Kiran, and V. S. Sreebalaji. "Micro structural characteristics and mechanical behaviour of aluminium matrix composites reinforced with titanium carbide." Journal of Alloys and Compounds 723 (2017): 795-801.
34. Zohari, Shokat, *et al*. "Application of spark plasma sintering (SPS) for the fabrication of *in situ* Ni–TiC nanocomposite clad layer." Journal of Alloys and Compounds 633 (2015): 479-483.

35. AlMangour, Bandar, Dariusz Grzesiak, and Jenn-Ming Yang. "*In situ* formation of TiC-particle-reinforced stainless steel matrix nanocomposites during ball milling: Feedstock powder preparation for selective laser melting at various energy densities." Powder Technology 326 (2018): 467-478.
36. Chawla, Krishan K. "Metal matrix composites." Materials Science and Technology (2006).
37. Training Sheet and Manual, Optomec Inc., Albuquerque, NM, 2003, pp. 3–4
38. Zheng, B. "Y, Zhou, JE Smugeresky, JM Schoenung, and EJ Lavernia." Metall. Mater. Trans. A 39 (2008): 2237.
39. B. Zheng, J.E. Smugeresky, Y. Zhou, D. Baker, and E.J. Lavernia: Metall. Mater. Trans. A, 2008, vol. 39A, pp. 1196–1205
40. Niino M, Hirai T, Watanabe R.J Jpn Soc Comp Mater 1987;13:257–64
41. Kawasaki A, Watanabe R.Ceram Int 1997;23:73–83.
42. Liu, Weiping, and J. N. DuPont. "Fabrication of functionally graded TiC/Ti composites by laser engineered net shaping." Scripta Materialia 48.9 (2003): 1337-1342.
43. Zheng, Baolong, *et al*. "The influence of Ni-coated TiC on laser-deposited IN625 metal matrix composites." Metallurgical and Materials Transactions A 41.3 (2010): 568-573.
44. Y. Xiong, J. E. Smugeresky, L. Ajdelsztajn, Julie M. Schoenung, Mater. Sci. Eng. A 493 (2008) 261
45. Schwendner, Katrin I., *et al*. "Direct laser deposition of alloys from elemental powder blends." Scripta Materialia 45.10 (2001): 1123-1129.

46. Kobryn, P. A., and S. L. Semiatin. "Mechanical properties of laser-deposited Ti-6Al-4V." Solid freeform fabrication proceedings. Austin, 2001.
47. A. Munir, U. Anselmi-Tamburini and M. Ohyanagi, 'The effect of electric field and pressure on the synthesis and consolidation of materials: A review of the spark plasma sintering method,' J. Mater. Sci., 41 [3] 763-777 (2006).
48. W. Chen, U. Anselmi-Tamburini, J. E. Garay, J. R. Groza and Z. A. Munir, 'Fundamental investigations on the spark plasma sintering/synthesis process: I. Effect of dc pulsing on reactivity,' Materials Science and Engineering A, 394 [1-2] 132-138 (2005).
49. X. Song, X. Liu and J. Zhang, 'Neck formation and self-adjusting mechanism of neck growth of conducting powders in spark plasma sintering,' J Am Ceram Soc, 89 [2] 494-500 (2006).
50. D. Chakravarty, H. Ramesh and T. N. Rao, 'High strength porous alumina by spark plasma sintering,' Journal of the European Ceramic Society, 29 [8] 1361-1369 (2009).
51. Consolidation and synthesis of materials by electric current activated sintering. Materials Science and Engineering, 63:127{287, 2009).
52. Tokita, M. "Mechanism of spark plasma sintering." Proc. of the Inter. Sympo. on Microwave, Plasma and Thermochemical Processing of Advanced Materials (1997): 69-76.
53. Thermal Technologies, LLC, 1911 Airport Blvd. Santa Rosa, CA. 95403 United States. Operating and Maintenance Manual, sps 10-3 10 ton edition, 2012.

54. Kim, Hoyeol, *et al*. "Laser engineered net shaping of nickel-based superalloy Inconel 718 powders onto AISI 4140 alloy steel substrates: Interface bond and fracture failure mechanism." Materials 10.4 (2017): 341.
55. Modest, M. F., J. Ready, and D. Farson. "Handbook of laser materials processing." (2001).
56. Salguero, Jorge, *et al*. "Application of Pin-On-Disc Techniques for the Study of Tribological Interferences in the Dry Machining of A92024-T3 (Al–Cu) Alloys." Materials 11.7 (2018): 1236.
57. D. Strzeciwilk, Z. Wokulski, and P. Tkacz, J. Alloy. Compd. 350, 256 (2003)
58. JCPDS card No: 87-0712 and 32-1383
59. Hull, D.; Bacon, D.J. Introduction to Dislocations, 4th ed.; Butterworth Einemann: Oxford, UK, 2001
60. B.E.Warren. X-Ray Di_raction, chapter 2, page 15. Dover Publications, 31 East 2nd Street, Mineola, NY 11501-3852, 1990
61. Young, Warren Clarence, Richard Gordon Budynas, and Ali M. Sadegh. Roark's formulas for stress and strain. Vol. 7. New York: McGraw-Hill, 2002.